NANO · MICRO small
www.small-journal.com

Peptide Nanophotonics: From Optical Waveguiding to Precise Medicine and Multifunctional Biochips

*Boris Apter, Nadezda Lapshina, Amir Handelman, Boris D. Fainberg, and Gil Rosenman**

Optical waveguiding phenomena found in bioinspired chemically synthesized peptide nanostructures are a new paradigm which can revolutionize emerging fields of precise medicine and health monitoring. A unique combination of their intrinsic biocompatibility with remarkable multifunctional optical properties and developed nanotechnology of large peptide wafers makes them highly promising for new biomedical light therapy tools and implantable optical biochips. This Review highlights a new field of peptide nanophotonics. It covers peptide nanotechnology and the fabrication process of peptide integrated optical circuits, basic studies of linear and nonlinear optical phenomena in biological and bioinspired nanostructures, and their passive and active optical waveguiding. It is shown that the optical properties of this generation of bio-optical materials are governed by fundamental biological processes. Refolding the peptide secondary structure is followed by wideband optical absorption and visible tunable fluorescence. In peptide optical waveguides, such a bio-optical effect leads to switching from passive waveguiding mode in native α-helical phase to an active one in the β-sheet phase. The found active waveguiding effect in β-sheet fiber structures below optical diffraction limit opens an avenue for the future development of new bionanophotonics in ultrathin peptide/protein fibrillar structures toward advanced biomedical nanotechnology.

1. Introduction

Nanophotonics is a wide field, based on basic physics, advanced optical materials, and nanotechnology. Optical waveguides,[1] which confine and guide light, are the basic components of multifunctional integrated chips combining linear, nonlinear optical, and electronic circuits in optical communication devices.[2,3] Other photonic applications are directed toward traditional medical analysis and disease monitoring.[4–6] Nowadays, biomedical and clinical researches are focused both on nano- and microtools and advanced methods of diagnosis, therapy, and surgery.[7,8] For these new developments the photonic technologies are crucial for rapid application of the emerging precise light theranostics in medical trials.[9,10] Light strongly influences basic biological processes that stimulates application of new biomedical photonic techniques exploiting diverse photochemical,[11,12] photobiological,[13] photothermal[14] effects and methods of light-induced therapies,[9] such as photodynamic and optogenetic therapies in addition to traditional optical bioimaging[15] and diagnostics.[16,17]

In this Review we present a new paradigm of emerging bio-optical physics and nanotechnology based on multifunctional bioinspired peptide nanomaterials toward new biomedical nanotherapy tools and implantable integrated optical biochips.[18] Biological structures, self-assembled from natural biounits such as amino acids, peptides, and protein biomolecules, known as the machinery of life, are the inspiration for the development of a new generation of man-made synthetic nanomaterials composed from chemically manufactured peptides and proteins. These bio-organic elementary scaffolds are self-organized into a broad range of supramolecular structures where building blocks are connected by weak, dynamic, and reversible noncovalent interactions.[19,20] Inherently biocompatible and biodegradable these new artificial nanostructural materials of biological origin opened the avenue for their wide applications in a few directions.[21,30] One of them

Dr. B. Apter, Dr. A. Handelman
Faculty of Engineering
Holon Institute of Technology
Holon 5810201, Israel
N. Lapshina, Prof. G. Rosenman
School of Electrical Engineering
Faculty of Engineering
Tel Aviv University
Tel Aviv 69978, Israel
E-mail: gilr@eng.tau.ac.il
Prof. B. D. Fainberg
Faculty of Science
Holon Institute of Technology
Holon 5810201, Israel
Prof. B. D. Fainberg
School of Chemistry
Tel Aviv University
Tel Aviv 69978, Israel
The ORCID identification number(s) for the author(s) of this article can be found under https://doi.org/10.1002/smll.201801147.

DOI: 10.1002/smll.201801147

is multiscale structures for translating biological design concept to similar hierarchical architectures mimicking unique combination of mechanical, chemical, transport, and optical properties of biological protein structures at nano- and microscale.[22,23] Another wide field is encoding of biological molecules, peptides, and proteins, and development of bioactive peptide materials for tissue engineering and regenerative medicine.[24,25]

The third direction is a new generation of bioinspired self-assembled synthetic peptide nanomaterials,[26–28] their nanotechnology,[29,30] physics, and engineering.[31–34] These materials of biological origin already showed potential applications in a variety of new fields,[35] such as piezoelectric energy harvesting devices and sensors,[36,37] displays and light-emitting devices,[38] superhydrophobic surfaces for self-cleaning,[29] composite reinforcement scaffolds,[39] flexible biodegradable electronics,[34] and more.

Recent research revealed in peptide nanostructures a unique set of optical properties, such as nonlinear optical,[44] electro-optical,[45] and optical waveguiding effects.[18,46,48] These previously unknown phenomena paved the way toward new physics of light propagation in biological and bioinspired nanostructures followed by nanotechnology of optical peptide waveguides. Such nanoscale light waveguides promise breakthrough applications toward biomedical theranostics and multifunctional optical implantable biochips where they are integrated with operating electronics. This new field of peptide nanophotonics[18,40–45] is the main goal of this Review.

We overview in this paper fundamental and applied photonic research of bioinspired peptide nanomaterials and highlight technological development of their applications in emerging field of peptide integrated optics.[18,40] Their exceptional optical properties such as broadband optical transparency from ultraviolet (UV) to near infrared (IR),[42,43] nonlinear optical,[44] and Pockles electro-optic[45] effects, combined with natural elongated morphology of self-assembled peptide nanostructures (nanotubes, nanofibers, and nanotapes) make them promising for optical linear and nonlinear waveguiding.[18,40,46–48] In contrast to well-known biomaterials' counterparts applied in implantable photonics, for instance, silk fibers, polymers, hydrogels, and more,[49–52] these peptide-based nanostructures have significantly higher refractive index ≈1.6 providing strong optical confinement of peptide optical waveguides.[18,41] Another key functional optical effect is a new phenomenon of intrinsic tunable visible fluorescence (FL) recently revealed in different bioinspired peptide nanostructures.[18,53,116,117]

The Review consists of several major parts. The introduction section describes the state-of-the-art and basic priorities of biomedical integrated optics, its related materials, and light-induced technological solutions in the advanced field of precise medicine. The emerging bio-optical physics and nanotechnology of bioinspired peptide multifunctional optical nanomaterials are considered in a few next sections where one of them covers nanotechnology of large peptide wafers, their high resolution patterning, fabrication of optical waveguides, and integrated peptide optical circuits. Another part gives a comprehensive review on basic linear and nonlinear optical properties of biological tissues and bioinspired peptide nanomaterials with specific emphasis on a new bio-optical effect of visible tunable fluorescence which appears under the peptide secondary structure refolding. The main chapter of this work is peptide integrated optics where a wide research of linear and nonlinear, passive and active optical waveguiding phenomena is considered in depth. This section

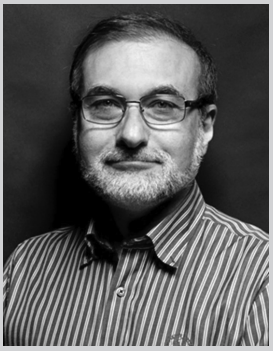

Boris Apter received his M.Sc. degree in electrical and electronics engineering from the Far-Eastern State Transport University, Khabarovsk, Russia, in 1982. He received his Ph.D. degree in physics from the State Research Institute of Optical and Physical Measurements, Moscow, Russia, in 1990. Since 2000, he has been at the Holon Institute of Technology, Israel. He is currently a senior lecturer and a head of the electro-optics laboratory at the Faculty of Engineering. His research interest fields include spatial light modulators, diffractive optics, optical tomography, wireless optical communication, nanophotonics, and plasmonics.

Amir Handelman received his B.Sc., M.Sc., and Ph.D. degrees in electrical engineering in 2008, 2011, and 2014, respectively, all from Tel Aviv University. In 2014 he joined the Faculty of Engineering in Holon Institute of Technology (HIT) as a lecturer and full-time faculty member. His research interest fields include bionanophotonics, light-matter interaction, nonlinear optics, optical communication, and waveguide structures.

Gil Rosenman received his M.Sc. degree in 1970 in experimental physics, Ph.D. degree in 1975 and Doctor of Science in 1989 both in Solid State Physics from Ural Polytechnic Institute (Yekaterinburg, Russia). In 1990 he joined the Faculty of Engineering, Tel Aviv University, where he is a full professor (1998) and incumbent of the Henry and Dinah Krongold Chair of Microelectronics (2010). His research interests include solid state physics, physics and engineering of ferroelectric materials. In the last 10 years he is involved in studies of basic physics of bioinspired nanomaterials, bionanodots, and peptide nanophotonics towards precise medicine and implantable lab-on-chip.

also demonstrates the first peptide optical circuits toward new development of lab-on-biochips in the direction of health monitoring, local diagnostics, and light-activated therapies. The last chapter describes active optical waveguiding in ultrathin β-sheet peptide fibers beyond the diffraction limit where intrinsic visible FL propagates as exciton–polariton quasiparticles. This future development opens up the avenue for a new physics and integrated optics in biological and bioinspired fibrillar nanostructures toward new medical light-induced tools and biophotonic theranostics nanotechnology.

2. Biomedical Integrated Optics and Related Materials

One of the critical problems in a new precise light-induced medical technology is delivering of the photonic flux to the targeted body location.[9–11,54] Basic physical processes of optical absorption and scattering under UV, visible, and IR light illumination of a human skin and tissues are limited by the depth of the light diffusion and penetration inside a human body.[55] The traditional approach to deliver the light both in vitro and in vivo as close as possible to the surface of biocells and human organs is to apply optical fibers[56,57] and endoscopes.[58] However, this technique limits the location of inspected and treated cells of internal organs near the surfaces only. The emerging trend to overcome the light penetration problem is development of implantable biomedical optical chips.[9,10,59,60] This new generation of biophotonic lab-on-chips encompassing both integrated optical and bioelectronic circuits can be exploited in a human body for a long period of time toward diagnosis, therapeutics, surgery and health monitoring.[10,61] Implantable biophotonic devices also serve as biosensors toward advanced healthcare for continuous monitoring and communication with a large set of human disease biomarkers and sensors.[62,63] For instance, fully integrated biochip platforms utilizing sensor devices with a life-time up to eight months enable continuous glucose monitoring.[64,65]

Optical waveguides[1,66] are the basic solution for multifunctional integrated implantable optical chips toward this new biomedical technology.[9,10,59] The waveguiding materials used for biomedical chips should exhibit specific figures of merit where the primary demand is their biocompatibilty and biodegradability.[2,10,54,63] Another basic requirement is their range of optical transparency in the visible–NIR range, since light in this spectral region directly affects tissues or excites materials that affect tissues.[14,15,17] To achieve lossless light guiding and its delivering into the targeted body location the optical biowaveguide should exhibit high optical confinement.[66] Such a basic condition is justified if waveguide's refractive index exceeds that of human tissues (for instance, the refractive index of the human skin is 1.38–1.44). These optical biomaterials should also have mechanical, chemical, and structural stability combined with sufficient flexibility, that can allow noninvasive and long-time integration of the biodevices with tissue.

Among optical waveguiding materials[10,51,52] silk fibers are the most attractive light waveguides for biophotonic chips due to their exceptional high mechanical properties combined with biocompatibility and wide optical transparency.[49,50] Such silk fibroin material can form thin films and subjected to 2D or 3D patterning through a soft lithography-based simple casting technique[67] for fabrication of diffraction gratings,[67] printed waveguides,[68] and implantable reflectors.[69] Biocompatible and biodegradable polymers are also good candidates for biophotonic devices.[57] Recently thin flexible bioabsorbable photonic waveguides made of synthetic Poly(lactic-*co*-glycolic acid) and poly(L-lactic acid) (PLA) polymers have been introduced.[70,71] Transparent and flexible implantable planar waveguides based on the PLA polymer extended the therapeutic depths in photodynamic, photothermal and optogenetic therapies.[57] Another group of biocompatible materials are hydrogel-based biopolymer materials. Optical hydrogel waveguides based on polyethylene glycol (PEG) and poly(vinyl-alcohol)[72] were used for light-controlled therapy, cell-based sensing and optogenetic synthesis in vivo in a mouse model with diabetes.[73]

3. Peptide Nanotechnology: Ordered And Patterned Peptide Nanostructures

3.1. Controlled Deposition and Patterning Methods for Aligning Peptide Nanostructures

Bioinspired materials are self-assembled from the synthetic biomolecular elementary building blocks, peptide and proteins. This natural process is governed by molecular recognition defining their morphological shapes and dimensions.[26,27,31] Among the endless variety of the peptide material morphologies, some of them have elongated architectures like nanofibers,[31] hollow rectangular microtubes,[74] rhombic rods,[75] and hexagonal hollow tubes[76] were studied. Intensive investigations of different peptide nanostructures and especially diphenylalanine (FF) nanotubes[27,76] revealed unique physical properties[29,31] such as piezoelectric effect,[77] semiconducting properties,[78] high mechanical rigidity[79] and stiffness,[80] quantum confinement,[81,82] nanoscale charge storage,[83] and more. These superior physical properties allowed to demonstrate promising applications of peptide nanostructures, such as autonomous motors,[84] piezoelectric power generators,[36,85] drug delivery systems,[86] and more. However chaotic distribution of self-assembled peptide functional nanounits remains the main obstacle for any development of peptide-based engineering of practical devices.

Several works reported and reviewed both top-down[87] and bottom-up[85,88] methods for controlling and patterning peptide nanostructures. These techniques included alignment of crystalline peptide nanowires by application of electric[89–91] or magnetic fields[76,92] (**Figure 1**a,b,d,e) as well as specific technique based on dynamic microfluidic control of peptide nanoassemblies' growth[93] (Figure 1c) and vapor deposition technology[31] (Figure 1f). Additional method of controllable self-assembly of peptide nanostructures were demonstrated by the use of evaporative dewetting solutions,[94] wettability modification,[95] and electrospinning.[96]

3.2. Peptide Nanophotonic Technology

Peptide nanophotonics is an emerging bio-optical field. Found fundamental optical effects such as linear (optical absorption (OA), visible fluorescence[18,53]), nonlinear optical

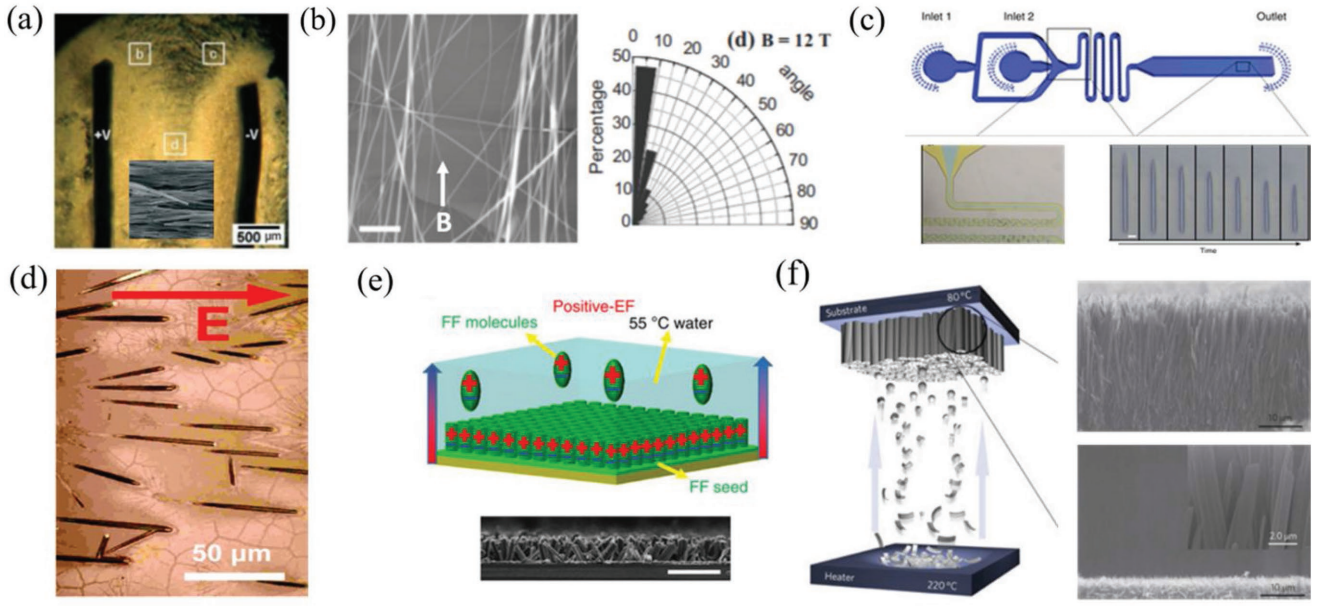

Figure 1. a) Alignment of peptide nanowires induced by electric field. Reproduced with permission.[89] Copyright 2007, John Wiley and Sons. b) Alignment of aromatic peptide tubes by strong magnetic fields. Reproduced with permission.[92] Copyright 2007, John Wiley and Sons. c) Dynamic microfluidic control of peptide nanoassemblies' growth. Reproduced with permission.[93] Copyright 2016, Springer Nature. d) Hexagonal tubular structures formed with horizontal external electric field. Reproduced with permission.[91] Copyright 2011, ACS. e) Alignment of uniform FF-microrods by application of in situ electric field during their growth. Reproduced with permission.[85] Copyright 2016, Springer Nature. f) Alignment of peptide nanostructures by vapor deposition technology. Reproduced with permission.[31] Copyright 2009, Springer Nature.

(second harmonic generation (SHG)),[44] Pockels' electroptic,[45] and optical waveguiding[18,40,46–48] in ultrashort di- and tripeptide nanostructures of different origin indicate highly promising applications of these new bioinspired nanomaterials for multifunctional bio-optical chips.[18]

Integrated photonics provided a wide development and revolutionized field of telecommunication engineering.[1,2] The implantable optical biochips exploit the same basic principles (**Figure 2**a–c). All optical devices are integrated at the same substrate having either a plain morphology or optical waveguiding units printed on a flat substrate.

We developed two different deposition methods of peptide tapes for waveguiding devices using deeply modified surface substrates[18] and nanofountain pen (NFP) direct writing.[41] The rectangular-shaped self-assembled tripeptide triphenylalanine (FFF)-wafer of a large area demonstrates a plain morphology (Figure 2e). Such a planar shape was prepared under controllable triphenylalanine (FFF)-monomer solution deposition on a glass substrate combined with a "pull-out" technique. The substrate was preliminary subjected to surface modification treatment providing a significant improvement of wettability. This technology enabled deposition of both 1D strips reaching 100 μm length and large FFF-wafers with dimensions over the range of length 5–100 μm, width 5–30 μm, and thickness 0.2–1.5 μm. At the next stage focused ion beam (FIB) was applied to pattern the FFF-wafer and fabricate FFF-peptide-based integrated optical devices such as 1 × 2 power Y-splitter (Figure 2f), Mach–Zehnder interferometer (Figure 2g), 1 × 2-power Y-splitter with input and output grating couplers (Figure 2h), and 1 × 2-power Y-splitter on large FFF-wafer (Figure 2i). We also demonstrated deposition of patterned Ga-electrodes on a single FFF-plate, indicating a new option of combination of peptide photonic devices with electronic circuits on the same biochip (Figure 2j).

Another option to control the deposition technology of peptide nanounits is to apply NFP lithography.[41,93] The developed NFP is a cantilevered microfluidic device that uses hollow glass or quartz capillaries with an aperture of a few hundred nanometers.[97,98] Figure 2l,m shows two FF-nanotubes deposited between two gold electrode as well as array of the tubes which could be used for light peptide biophotonic waveguides.[41]

4. Bioinspired Peptide Nanostructures: Basic Linear and Nonlinear Optical Properties

Bioinspired materials are supramolecular structures. Their self-assembly process governed by biomolecular recognition, passes several different stages. At the first stage original monomer biomolecules are self-assembled into nuclei of a critical size which can be recognized as nanodots (**Figure 3**a).[81,99] These primary seeds are organized at the next stages into large supramolecular nanoensembles[27] with specific ordering of peptide/protein secondary structure.[100] The two common types of biological secondary structures are α-helices and β-sheets.[101,102] Under certain environmental conditions the primary bioclusters self-organized into native metastable α-helical structure allow refolding of the thermodynamically stable β-sheet topological motif.[103,104] Such a stability is kept by reconstructed strong hydrogen-bonded intermolecular interactions.[105,106] Having identical biochemical core amino acid compositions of peptide/protein structures, these two fundamental biological phases exhibit completely different biomedical[107,108] and physical properties.[18,53,109]

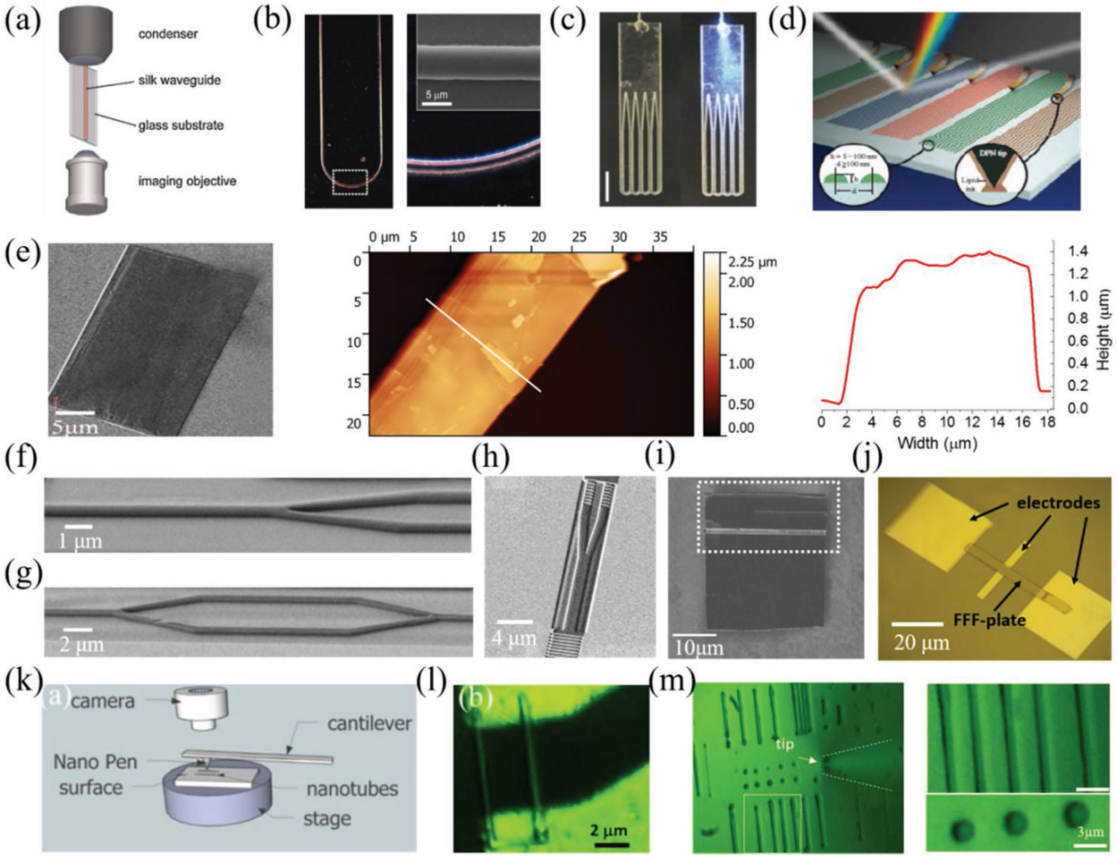

Figure 2. a) Schematic setup used for imaging and analyzing silk waveguides. b) Printed silk waveguide and its higher magnification view of the curved feature highlighted by the dashed box. Reproduced with permission.[68] Copyright 2009, John Wiley and Sons. c) Planar waveguide demonstrations. Reproduced with permission.[57] Copyright 2016, Springer Nature. d) Dip-pen nanolithography used to fabricate lipid multilayer gratings. Reproduced with permission.[62] Copyright 2010, Springer Nature. e) Scanning electron microscopy, SEM (left); atomic force microscopy (AFM) images (middle); AFM profile of FFF-planar wafer of dimensions 15 μm × 34 μm × 1.4 μm. f) 1 × 2 power Y-splitter. g) Mach–Zehnder interferometer. h) 1 × 2 power Y-splitter with output grating coupler. i) 1 × 2 power Y-splitter on large-scale FFF-wafer. j) Ga-electrodes deposited on a single FFF-tape by FIB. Reproduced with permission.[18] Copyright 2017, John Wiley and Sons. k) Nanofountain Pen (NFP) setup. l) Optical microscope image of two FF nanotubes deposited by NFP lithography between two gold electrodes. n) FF-fibers and spheres deposited by NFP. Reproduced with permission.[41] Copyright 2017, John Wiley and Sons.

Among a variety of figures of merit of photonic materials applied for light waveguiding, OA, FL, refractive index, nonlinear optical phenomenon of SHG and electro-optical effect are the key properties enabling to develop peptide multifunctional optical circuits and integrated biochips.[1,2,9,10]

4.1. Linear Optical Properties of Peptide Nanostructures: Optical Absorption and Visible Fluorescence in Peptide/Protein Nanostructures

Original electronic structure of elementary monomer biomolecules (amino acids, peptides, proteins) does not allow to observe OA and FL in the visible region[111,112] except the unique FL protein of the jellyfish *Aequorea Victoria* and its homologues, which displays strong optical absorbance in the blue region and FL in the green spectral region with a quantum yield ≈0.8.[110] These optical features are widely used for direct monitoring of basic biological processes both in vivo and in vitro in cells and tissues in biomedical research, theranostics,[111,112] and new bio-optical applications such as implantable biochips.[9]

The ultrashort aromatic FF, FFF, and aliphatic dileucine (LL) (Figure 3b,c), self-assembled into elongated nanostructures, can be used for light waveguides. They are optically recognized both in OA and FL spectra according to their core phenylalanine and leucine amino acids. Original FF-, FFF-, and LL-peptide nanoensembles studied by circular dichroism method show that in a native, virgin state they are self-assembled into α-helical-like peptide secondary structure (Figure 3p–r). Measurements of OA spectra of the peptide nanostructures allow to define the region of their optical transparency. Aromatic FF- and FFF-peptide structures regardless of both their architecture/morphology (tubes, fibers, spheres, tapes) and peptide secondary conformation (α-helices or β-sheets) demonstrate in UV region the same OA and FL optical signatures, 250–290 nm (Figure 3e–g,l,n), which is ascribed to benzoic rings of phenylalanine, F-amino acid.[111] This biomolecular optical signature of F-amino acid was found in all F-based self-assembled nanostructures: FF-dots,[99] FF-nanotubes,[29] FF-spheres,[53] FF-fibers,[42] and FFF-tapes[18] (Figure 3a–d, h–k). It should be noted that aliphatic leucine-based LL-dipeptide native nanotubes do not demonstrate OA

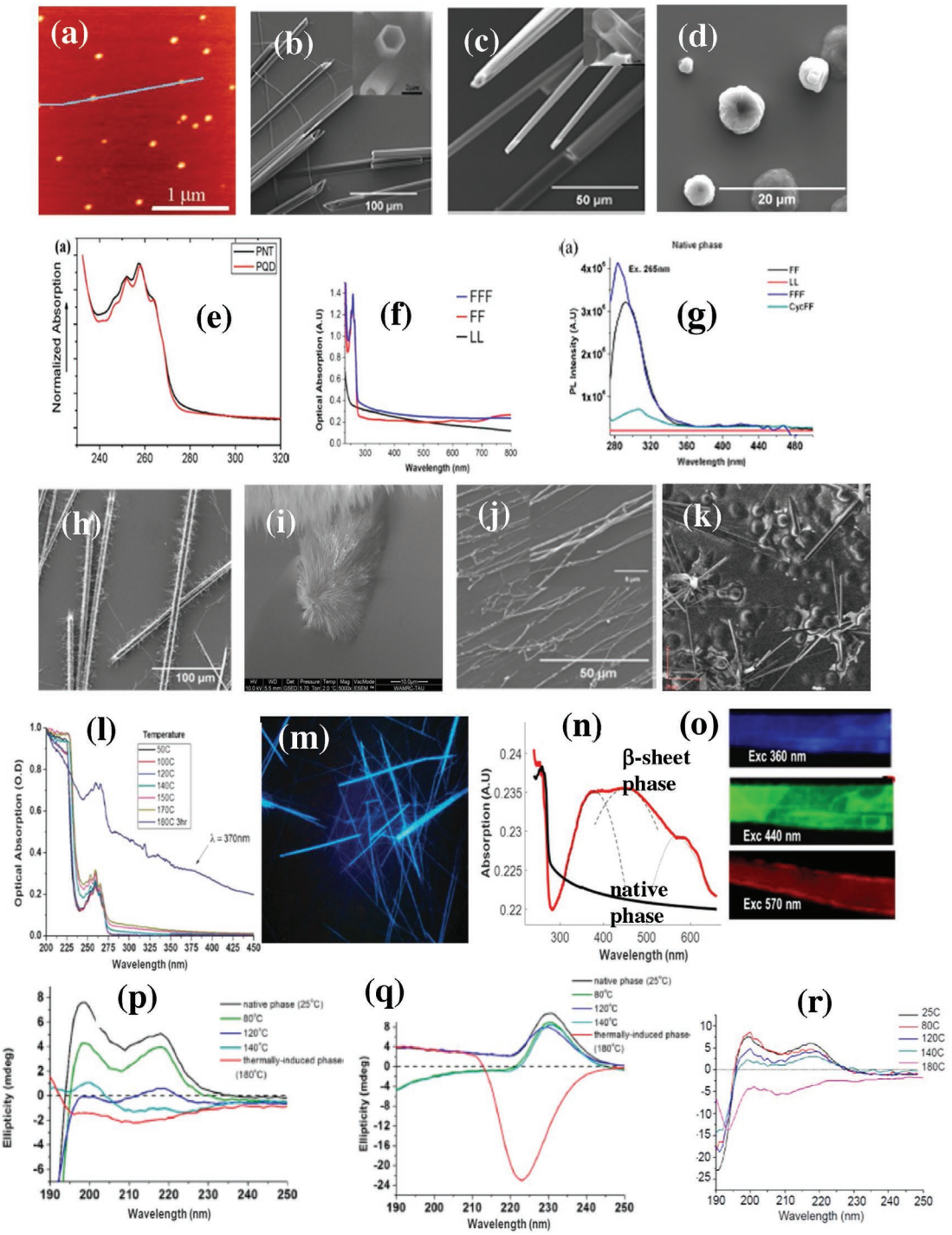

Figure 3. a) AFM image of FF-peptide nanodots, average dimension 2.1 nm. Reproduced with permission.[99] Copyright 2010, American Chemical Society. b) SEM image of native FF-peptide nanotubes. c) SEM image of native LL-peptide nanotubes. d) SEM image of native FFF-peptide spheres. e) OA of native FF-dots and FF-nanotubes. OA is found in the region 250–280 nm. f) OA of native FF- and FFF-spheres. OA is in the region 250–280 nm. g) FL of native FF- and FFF-spheres. UV FL peak at ≈290 nm. No FL is for native LL-peptide nanotubes. h) SEM image of FF-fibers after thermally induced reconformation of peptide secondary structure from native phase to β-sheet. i) High resolution SEM image of FF-fibers, β-sheet secondary structure. j) SEM image of LL-fibers after thermally induced reconformation of peptide secondary structure from native phase to β-sheet. k) SEM image of FFF-fibers after thermally induced reconformation of peptide secondary structure. l) OA of FF-nanostructures during gradual heating resulting in thermally induced reconformation of peptide secondary structure. m) Blue FL in β-sheets phase of FF-fibers. n) OA of FFF-tapes in native structure (black color graph) and in thermally induced β-sheet (red color graph). o) Multicolor tunable FL of FFF-tapes with β-sheets peptide secondary structure. Reproduced with permission.[99] Copyright 2010, American Chemical Society. p–r) Circular dichroism exhibiting in FF-, LL-, FFF-nanostructures thermally induced reconformation of peptide secondary structure from native phase to β-sheets. d,h,p–r) Reproduced with permission.[53] Copyright 2016, American Chemical Society. Available at: https://pubs.acs.org/doi/abs/10.1021/acs.langmuir.5b02784. Further permissions related to the material excerpted should be directed to the American Chemical Society.

and/or FL-effect in this UV spectral interval (Figure 3f,g).[53] Studies of OA in leucine amino acid-based films show OA in the far UV region only at 120–190 nm.[111–113] Thus both F-aromatic and L-aliphatic-based nanostructures in their native states are transparent in a wide optical region covering near UV, visible, and NIR regions (Figure 3). FL effect for all aromatic compositions is observed in UV region, $\lambda \approx 290$ nm.[53,196]

Deep and unexpected modification of optical properties of aromatic and aliphatic nanostructures[18,53,114] were revealed under thermally mediated refolding of the peptide secondary structure from native α-helical state to β-sheets[53] (Figure 3p–r). The experimental data (Figure 3l–o) exhibit the appearance of significant changes of OA and FL in the visible region for all studied ultrashort peptide structures regardless of their composition. This new biophotonic phenomenon is induced by biological transformation of peptide secondary structure. It was found that native FF- and LL-nanotubes and FFF-nanospheres are undergone to irreversible phase transition in the temperature range of 120–180 °C.[31] The reconformation of the peptide secondary structure from α-helical to β-sheet structure (Figure 3p–r) leads to pronounced morphological changes in the hollow FF- and LL-nanotubes[53,114,115] and FFF-spheres[53] (Figure 3b–d,h–j). They are gradually smashed, passing through a glass-like state[115] and finally are grown into very thin elongated fibrillar structures of 10–100 nm diameter.[53] The effect is accompanied by irreversible reconstruction of the covalent intramolecular hydrogen bonds of α-helical secondary structure to a new type of intermolecular hydrogen bonds of β-pleated sheets.[18,53,114]

This reconformed peptide supramolecular fiber architecture exhibits deep modification at all levels (molecular, morphological, peptide secondary structure, electronic, optical and more) providing new physical properties, which are not observed in the original biomolecule monomers and their self-assembled native nanostructures.[18,31,53,114] In the native α-helical phase, FF-, LL-nanotubes and FFF-nanospheres possess asymmetric structure and demonstrate unique physical properties such as piezoelectric,[77] nonlinear optical[44] and electro-optical[45] effects. In the thermally induced phase, these phenomena disappear as a result of the newly reassembled centrosymmetric structure. All these refolded FF, LL and FFF fiber nanostructures acquire the same β-sheet secondary arrangement, followed by profound modification of the native electronic properties resulting in the visible FL (Figure 3l–o).

Found in ultrashort di- and tripeptide nanofibers visible FL effect has the same physical origin as FL effect revealed in PEGylated peptide PEG-F6 and its derivatives,[116,117] nonaromatic biogenic and synthetic peptides,[118] amyloid fibrils[119,120] and recently in natural silk fibrils.[121] This biophotonic effect is considered as an optical signature of β-sheet peptide secondary biological structures (Figure 3p–r). It is ascribed to noncovalent hydrogen bonds interconnecting the β-strands into β-sheet structure and creating a dense network of intrinsic visible fluorescent dyes.[53,116–120,122]

These results open the avenue for multifunctional peptide integrated optical circuits, where both waveguiding modes, passive and active, are observed.[18]

4.2. Nonlinear Optical Properties of Biological and Bioinspired Structures

4.2.1. Elementary Symmetry of Biological and Bioinspired Peptide Nanostructures and Their Basic Physical Properties

Biological systems have a common feature of intrinsic organization into chiralic dissymmetric structures revealed by Pasteur.[123] Natural asymmetry enable to observe in the biological systems basic physical phenomena described by tensors of the 3-rd rank such as piezoelectric, nonlinear optical and electro-optical effects.[124] Both biomolecules and biomolecular crystals contain neither an inversion of center nor mirror symmetry.[125] The proteins are composed of 20 known natural amino acids, and 19 of them possess asymmetric structure exhibiting piezoelectric properties.[126] Piezoelectricity[127–129] and SHG are observed in a large range of biological systems and tissues such as proteins, biopolymers, polysaccharides, pineal glands, human collagen, bones, tendon, muscles and more.[130–133]

Bioinspired peptide-based nanostructures self-assembled from synthetic biomolecules adopt highly ordered nonsymmetrical arrangement,[134] as well as many other bio-organic and organic compounds.[133,135] Conducted structural studies[31,115] revealed that aromatic FF nanotubes in the native phase have noncentrosymmetric hexagonal P_{61} space group symmetry. Another LL peptide nanotubes[53] are also described by noncentrosymmetric space group P_{2121}.[134,136] These observations were deduced from XRD measurements.[115] Studied peptide nanostructures dramatically change their acentric crystalline ordering and becomes centrosymmetric[31,115] after this thermally induced reconstructive biological α-helix/β-sheet phase reconformation.[18] Original noncentrosymmetric structure of these bioinspired materials enabled observation of piezoelectric,[77,115,136] nonlinear optical[44] and electro-optical effects.[45]

4.2.2. Nonlinear Optics in Biological Materials and Its Application to Biomedical Research and Diagnosis

SHG is a basic nonlinear optical effect, which stems from electron–photon interaction in crystals without center of symmetry.[137] Because of nonsymmetrical structure the optical wave generates nonlinear electronic polarization, which oscillates with twice the fundamental frequency. The SHG effect is an emerging field of biomedical microscopy, bioimaging and diagnostics for a wide range of diseases.[138,139] For example, SHG microscopy was applied as a cancer diagnostic tool[140,141] to probe the structural differences in the extracellular matrix of normal stroma, benign tumors, endometrioid tumors, and more.[142] Furthermore, SHG microscopy was used to identifying articular osteochondrosis in pigs,[143] and as an early diagnostic tool for corneal related diseases[144] and imaging of collagen distributions in human sclera.[145] SHG microscopy enabled to observe structural changes in optic nerve head structure[146] and for imaging skin damages.[147]

Collagen is the main structural protein in connective tissues, such as tendon, skin, cornea and sclera.[148] Its SHG images in various tissues are presented in **Figure 4**. The basic structure

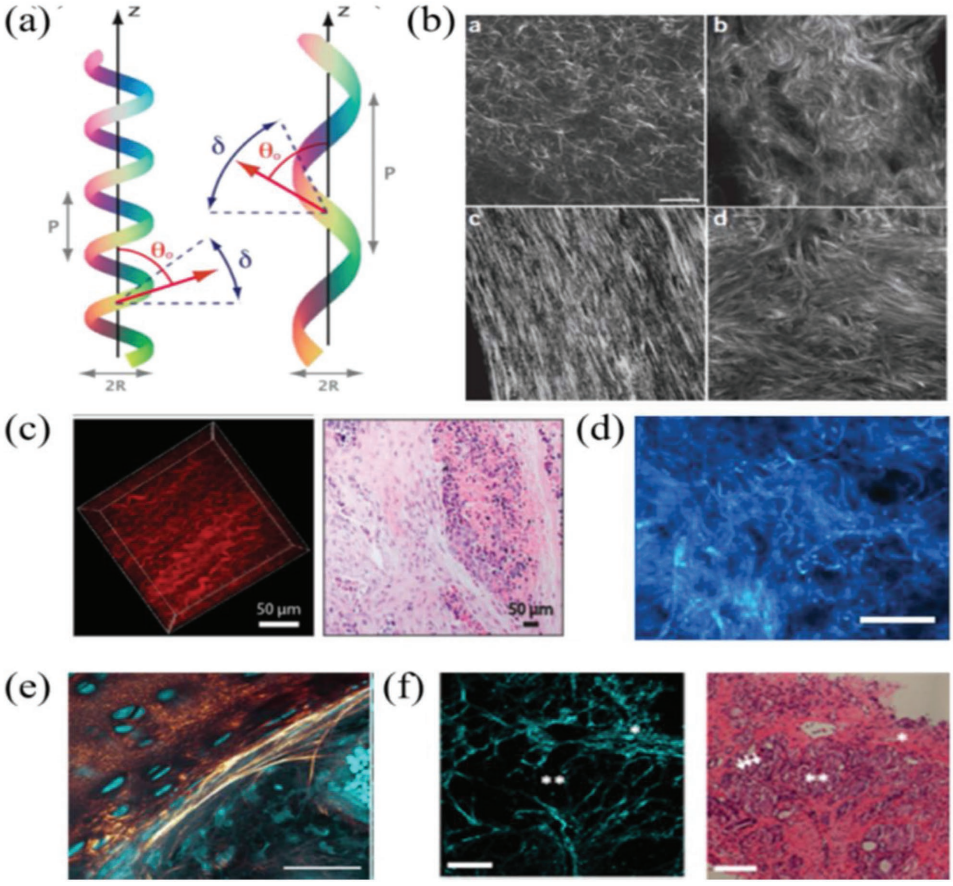

Figure 4. a) Schematic view of single helix of myosin (left) and collagen (right). Reproduced with permission.[148] Copyright 2007, Optical Society of America. b) SHG imaging of collagen tissues of self-assembled (clockwise, top-left: collagen gel; mouse dermis; mouse bone; human ovary). Reproduced with permission.[139] Copyright 2012, Springer Nature. c) SHG images of representative and ovarian tumors obtained at 890 nm excitation, and its histology image. Reproduced under the terms of the CC-BY 4.0 license (https://creativecommons.org/licenses/by/4.0/).[142] Copyright 2017, the Authors, Published by BioMed Central Ltd. d) Collagen distributions in SHG images of a piece of human sclera. Reproduced under the terms of the CC-BY 3.0 license (https://creativecommons.org/licenses/by/3.0/).[145] Copyright 2016, the Authors, Licensee IntechOpen. e) Image of cartilage canal with a boundary of collagen fibers. Cyan: two-photon-excited fluorescence (TPEF); glowing red: second harmonic generation (SHG). Strands of high SHG intensity, indicating collagen fibers, appear to originate in the interior of the canal and align at the canal margin. Reproduced under the terms of the CC-BY 4.0 license (https://creativecommons.org/licenses/by/4.0/).[143] Copyright 2017, BioMed Central Ltd. f) SHG images of collagen alignment in malignant prostate biopsy, and its histological images of fused glands occupied by cancer cells. Scale bar is 100 μm. Reproduced with permission.[141] Copyright 2016, John Wiley and Sons.

of collagen fibril is a triple helix (Figure 4a) composed of three protein chains, which build their noncentrosymmetric C_6 crystalline ordering that allows observing SHG.[149,150] In the past years, wide studies were conducted on the molecular structure of collagen and its second-order response.[151–156]

An important conclusion that was derived from studying the second order optical response of collagen was that it can be modeled by an ensemble of 1D individual molecules elongated along a helix structure with molecular distribution in a shape of a cone.[149] The molecular orientation of noncentrosymmetric biocrystals in the microscopic frame was detected by polarization resolved nonlinear microscopy.[157]

4.2.3. SHG and Molecular Dipole Orientation in Peptide Bioinspired Supramolecular Nanostructures

Second-order nonlinear optical response was found in a few peptide nanostructures: FFF-peptide nanotapes (PNTp), peptide nanospheres (PNS),[44] and FF-PNT.[158] The scanned map presented in **Figure 5** shows that FFF-PNTp radiates at twice the fundamental frequency, where the red and yellow colors present SHG intensity.

The second-order nonlinear optical response to an incident optical field of the fundamental frequency stems from the dipole moment oscillation of every biomolecule with a double frequency. Every light induced dipole oscillates at its own phase and generates a specific dipole radiation pattern that depends on its orientation. For a material containing N molecules all the dipoles in the material oscillate with the same phase and then the radiated waves constructively interfere by a coherent summation.[155] The highest magnitude of this interference is observed when the incident optical polarization is parallel to the molecular transition dipole moments.[149] In this manner, by rotating the electric field clockwise at an angle ψ relative to the laboratory axis, and measuring for each angle the nonlinear response, the molecular distribution can be probed and the direction of the emitted molecular dipoles can be

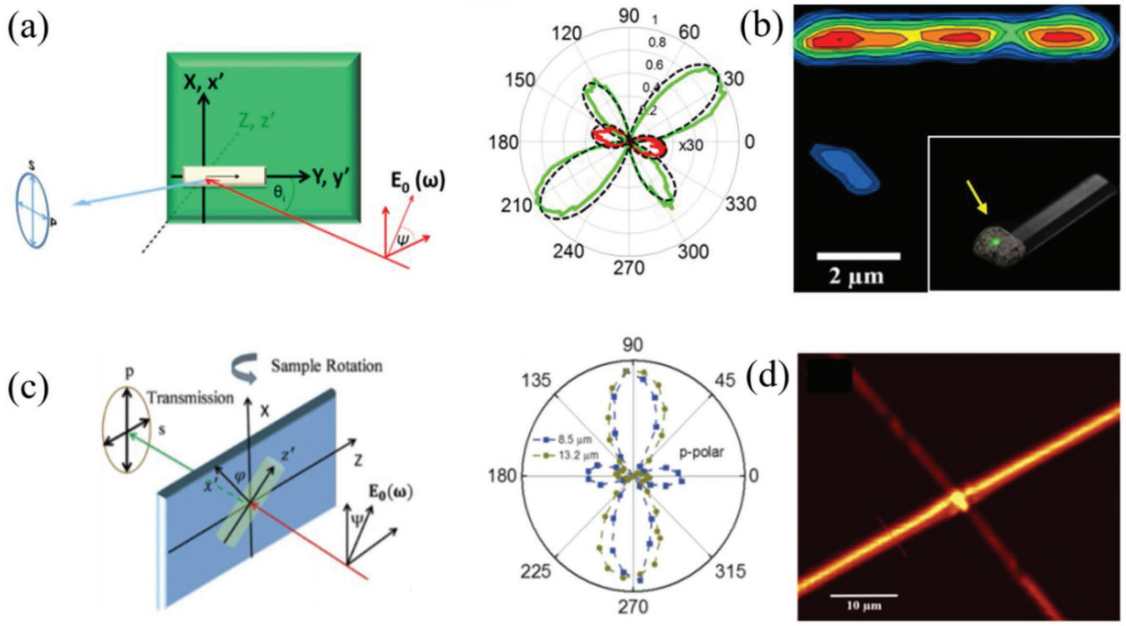

Figure 5. a) Definition of the coordinate systems in the laboratory frame (*X*,*Y*,*Z*) and in the microscopic frame (*x*′,*y*′,*z*′) for FFF-PNB, and simulated (dash line) and experimental ($I_p^{2\omega}$ green line, $I_s^{2\omega}$ red line) SHG polarimetric responses of FFF peptide PNP aligned along Y-axis. b) SHG imaging of FFF PNB. Inset shows a photo of the frequency conversion (IR-to-green light) from a bundle of FFF peptide nanotapes. c) Schematic of the SHG setup for FF-PNT and experimental SHG polarimetric response from two FF-PNTs with different outer diameters for p-polarization. Reproduced with permission.[158] Copyright 2017, Royal Society of Chemistry. d) SHG imaging of FF PNT. a,b,d) Reproduced with permission.[44] Copyright 2013, John Wiley and Sons.

determined.[149] Such a method is known as SHG polarimetry. The SHG polarimetric responses of FFF-PNTp and FF-PNT were measured with respect to the laboratory axis, as presented in Figure 5.

The orientation of the induced biomolecular dipole of FFF-PNTp was evaluated by observation of SHG intensity for two FFF-PNTp units when one of them is oriented in a direction parallel to the incident light polarization and another one is normal (Figure 5b). We observed that the SHG response intensity is larger by two orders of magnitude for the FFF-PNTp oriented along light polarization compared to its FFF-PNTp perpendicular counterpart.[44] This result allows to conclude that

a. FFF-nanoassembles self-organized into elongated morphology have homogeneously oriented native biomolecule dipole moments along the tapes which is the direct evidence of their native α-helical-like peptide secondary structure.
b. SHG light wave generated in FFF-tapes preserves the fundamental wave original polarization and allows to use such elongated structures as SHG waveguides which are promising for application in implantable biochips.

4.2.4. Electro-Optic Effect in Peptide Nanostructures

Another basic and widely used physical phenomenon ascribed to noncentrosymmetric peptide structures is the linear electro-optic (EO) effect.[159] Materials possessing this property change their refractive index linearly as a response to an externally applied electric field.[160] Recently, the effective EO coefficients of self-assembled peptide nanostructures of FF-PNT and FFF-PNTp[45] were measured by using Pockels linear electro-optic microscope. The EO coefficient of the FFF-PNTp are 3.8 pm V^{-1} along the tape, and 1.4 pm V^{-1} perpendicular to it which are close to inorganic EO barium borate crystals. The EO coefficients of the FF-PNT are as high as in ferroelectric crystal lithium niobate and reach 32 pm V^{-1} along the tube, and 3.5 pm V^{-1} perpendicular to it. These data indicate that peptide waveguides structures could be applied in multifunctional peptide integrated optical chips as EO biocompatible probes and biomedical sensors.

5. Peptide Integrated Optics

Integrated optics is a term that refers to the integration of a variety photonic components on a common planar substrate such as beam splitters, couplers, interferometers, electro-optic modulators, nonlinear optical converters, and more.[1] The key elements of these components are optical waveguides guiding the light in the photonic circuits, and perform transmission, distribution, modulation and processing of optical signals. Optical integrated devices traditionally utilizes diverse dielectric, ferroelectric, glass, silicon, and organic materials.[1,2,161,162]

There are two sorts of optical waveguides, passive and active. Passive waveguides directly guide the laser light to the output end through optical transmission window whereas active waveguides absorb the input laser light and guide the excited FL light waves. In this section we consider a new generation of integrated photonics based on bioinspired tubular and planar 1D- and 2D-peptide multifunctional linear and nonlinear waveguides.

5.1. Passive Linear and Nonlinear Peptide Waveguides and Integrated Circuits

5.1.1. Linear Passive Waveguiding in Peptide Elongated Structures

Wide optical transparency observed in native bioinspired peptide nanostructures,[42,43] their dimensions and shapes (Figure 3) make them promising for passive light waveguiding in near UV–visible–NIR region.[18,41] One of the main issues of any passive waveguiding structure is the problem of effective coupling of the input light beam to a guiding core. Traditional techniques in integrated optics are based on end-butt[163–165] or prism-coupling.[166–168] These methods cannot be applied for micro- and nanometer scale peptide/protein fiber-, tube-, or platelet-like waveguides where the experimental setup[18,41] applies a light beam which is incident normally to the peptide waveguide axis and sharply focused on its end. In such a case the excitation of guided modes[18,41] can be attributed to unpredictable, noncontrollable scattering of the incident beam from the waveguide irregularities, such as ends or edges of the peptide guiding core. This coupling/waveguiding/out-coupling mechanism has been experimentally demonstrated in several studies for various organic waveguiding structures.[169–172]

We studied light propagation in passive peptide waveguides of different geometries: FF-hollow tubes and FFF-planar tapes. **Figure 6**a exhibits the light waveguiding through peptide FF-nanotube deposited on a glass substrate. Incoming laser beam at the wavelength 633 nm is incident normally to the tube axis at different positions along the tube. It is shown that the incoming light is partly scattered and effectively coupled to the guided mode only when the laser beam is focused on one end of the peptide tube.

Computer simulations of this coupling/waveguiding/out-coupling mechanism were performed by the use of Finite Difference Time Domain Method (FDTD, Lumerical Inc.[173] Figure 6b). The simulation model consists of hollow, hexagonal, dielectric peptide tube placed on a glass substrate. Focused Gaussian beam incidents normally to the tube axis through the glass substrate. Both, the simulation and the experiment, demonstrate light coupling at the one end of the FF-tube followed by its propagation along waveguide axis and out-coupling at the other end of the waveguide.

Similar experiments and simulations were also performed for thin planar peptide FFF-tapes[18] (**Figure 7**). The focused beam of a white light emitting diode (LED) is normally incident on the tape and scanned along its axis. The waveguiding effect was observed when the light spot illuminates one end of the tape (Figure 7b,d), indicating light coupling to the waveguide. When the light spot illuminates the central, uniform part of the peptide tape, the waveguiding effect was not observed. Figure 7e–h shows the results of FDTD simulation of light propagation in FFF-peptide tape. The color maps represent 2D-distributions of electric field intensities of the light propagation in the three orthogonal central sections of the tape, confirming the light confinement inside it. Similar results (Figure 7i–l), consistent with the FDTD simulations, were observed in planar, wide FFF-peptide tape In this case, depending on light coupling conditions, the light beam can

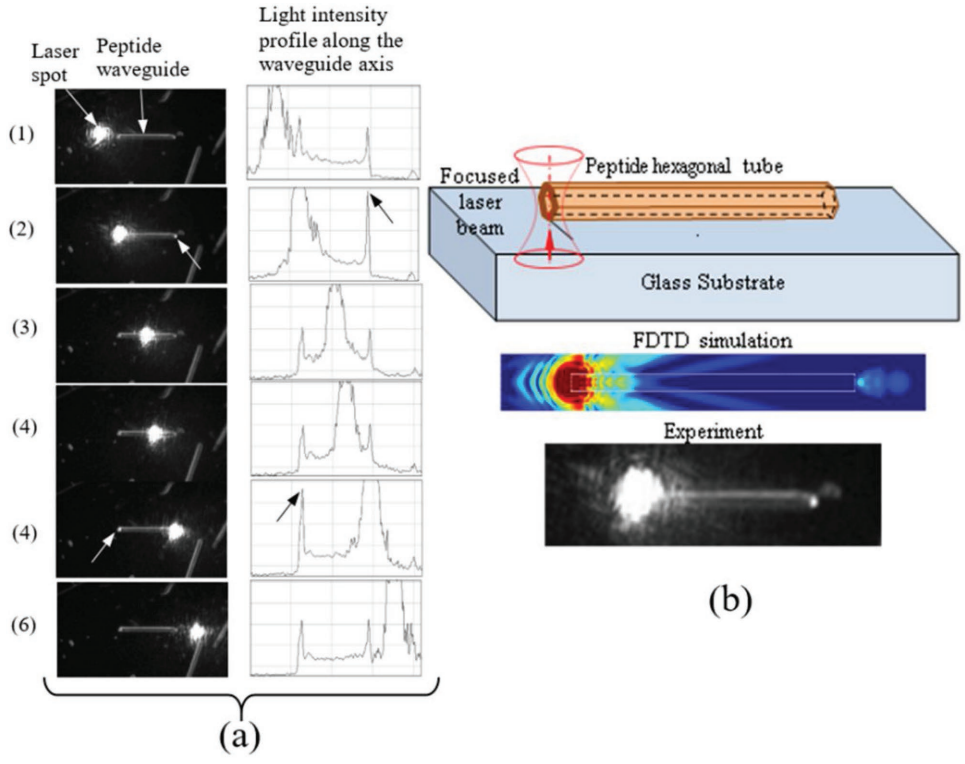

Figure 6. Light propagation along FF-peptide tube waveguide. a) Scanning laser spot along the tube. Only when the laser beam is focused on the left (2) or right (4) ends of the peptide tube, the incoming light is partly scattered and coupled to the guided mode. b) Comparison between FDTD simulation and experiment.

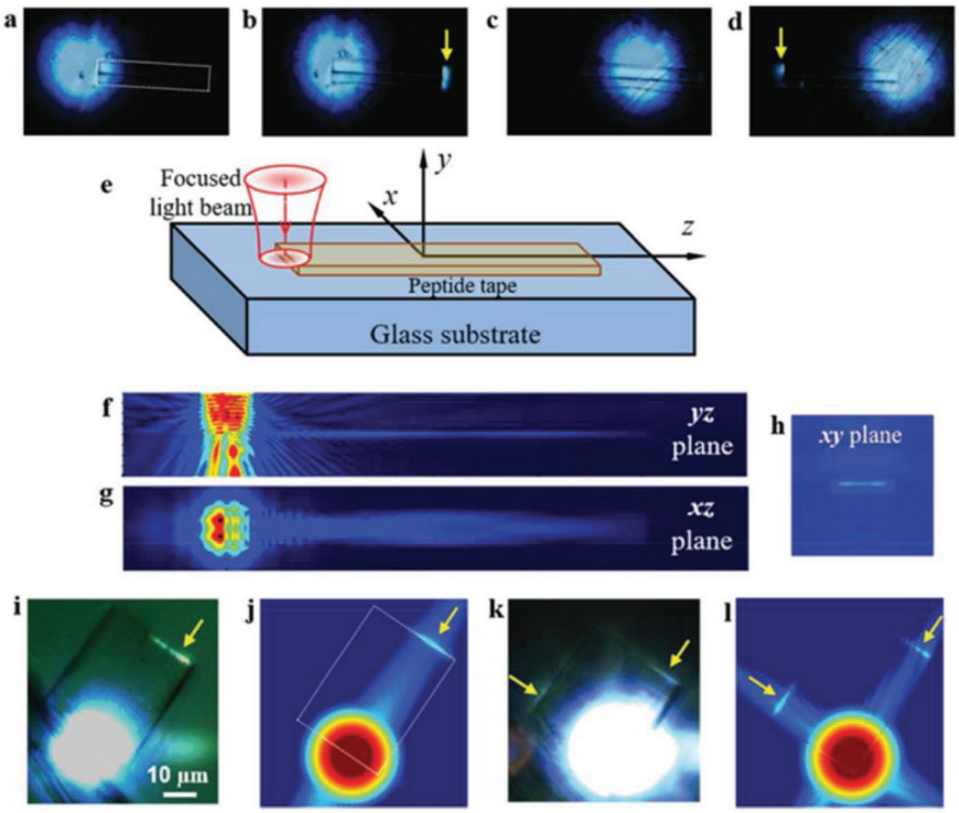

Figure 7. Passive optical waveguiding in thin planar FFF-peptide tape and wafer. a–d) The waveguiding effect is observed when the light spot is coupled to the end of the peptide tape. The coupling mechanism is attributed to the scattering of the normally incident focused light beam at the ends of peptide tape. e) Simulation configuration of passive waveguiding in FFF-tape according to the experimental setup. f–h) The simulation shows that even under normally incident illumination light can propagate along the peptide tape. i) Passive optical waveguiding in FFF-peptide wafer. j) Simulation of such a phenomenon is in a good agreement with the experiment. k) 2D passive waveguiding. Illumination by white LED at the corner of the peptide wafer leads to 2D passive waveguiding. l) Simulation of 2D passive waveguiding. Reproduced with permission.[18] Copyright 2017, John Wiley and Sons.

propagate either in one direction (Figure 7i) or in two orthogonal directions (Figure 7k), indicating 2D waveguiding effect.

It should be noted, that studied and tested peptide structures exhibit good optical confinement and pronounced waveguiding properties since the refractive index of these peptide structures ($n \approx 1.6$)[18] is higher than that of air environment and glass substrate ($n = 1$ and 1.52 correspondingly).

The effective in- and out-coupling of a light beam in passive peptide waveguides was theoretically studied and experimentally implemented by the use of diffraction grating couplers, patterned by FIB in FFF-peptide tapes.[18] In this study a planar, peptide-based Y-splitter designed for the blue spectral range was fabricated by incorporating diffractive grating coupling elements using FIB tool at all of its three ports (**Figure 8**a,b). The FDTD simulations were performed by the use of the grating coupler realistic 3D model imported to the FDTD simulation software from atomic force microscopy (AFM) image data (Figure 8a). Effective light coupling, waveguiding, splitting, and out-coupling under broadband white LED illumination of the input grating was demonstrated. Two blue light spots observed at the output gratings (Figure 8c) indicate selective wave coupling through grating elements, acting also as an optical filter. The FDTD simulations show a good agreement with the experimental data (Figure 8c,d).

5.1.2. Nonlinear Passive Waveguiding in FF-Peptide Nanotubes

Development of integrated nanophotonic devices has accelerated the research of nonlinear optical effects in organic nanowires and nanotubes.[174,175] These new materials such as 3-methyl-4-methoxy-4′-nitrostilbene self-assembled into hexagonal microprisms[176] and 2,7-diphenyl-9 H-fluoren-9-one microfibers[177] have been already introduced as effective nonlinear photonic waveguides. As shown in the former sections, both biological fibers[139,142,145] and bioinspired peptide nanostructures FF-PNT and FFF-PNTp exhibit nonlinear second order optical response,[31,44] and thus make them possible to guide second harmonic frequency wave in their noncentrosymmetric clad both for medical diagnostics[4,139] and device applications.[48] To test their waveguiding property, vertically aligned FF-PNT were fabricated by the breath figure method.[178] The FF-solution was rapidly evaporated, leaving microscale FF-PNT scaffolds. The measurements of the propagating light through normally oriented FF-PNT were performed for two light frequencies: fundamental wavelength, $\lambda = 800$ nm and SHG frequency at the wavelength of $\lambda_{SHG} = 400$ nm.[48]

Simulation of these FF-ultrashort tube-like structure under plane wave excitation shows that the ultrashort FF tubes acts

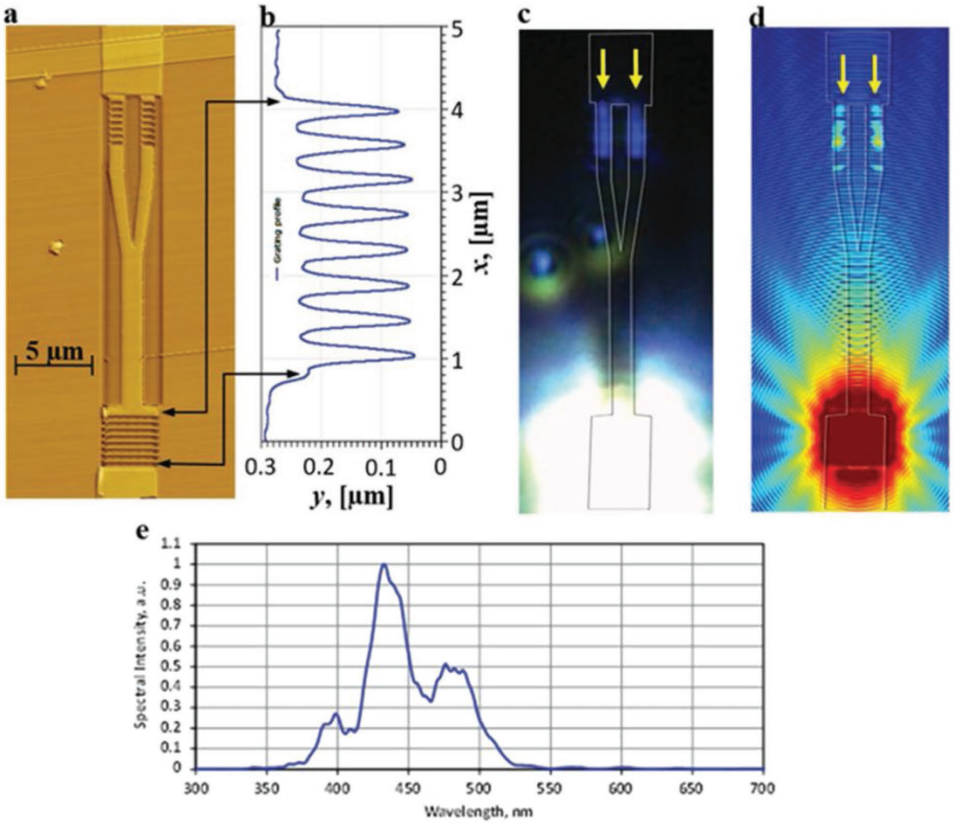

Figure 8. Peptide-based 1 × 2-power Y-splitter with grating couplers at all three ports. The couplers were designed for the blue spectral range. a) AFM image of FFF-based 1 × 2 power Y-splitter with grating couplers in its channels fabricated by FIB tool (main channel: ≈1.54 μm width, two split channels: ≈1.1 μm width). b) Height profile of the input grating (period ≈0.4 4 μm, maximum height ≈180 nm) that was milled by FIB. c) Experimental observation (optical microscopy image) of the efficient optical coupling, waveguiding and out-coupling in the 1 × 2 optical-power Y-splitter under white LED illumination of the input grating. Two elongated blue spots observed at the output ports indicate selective wavelength coupling and out-coupling by the grating couplers. d) Simulation of optical 1 × 2-power Y-splitter with grating couplers at its channels shows a good agreement with the experimental results. e) Calculated spectral intensity at the output gratings (spectral response of the device). The maximum intensity of out-coupled light is achieved in a blue light region that is consistent with presented experimental data. Reproduced with permission.[18] Copyright 2017, John Wiley and Sons.

like a diffractive multifocal lens (**Figure 9**a,b). It was found that the fundamental excitation light (λ = 800 nm) passes through the hollow core of the ring and focuses at two points along the *Z*-axis. In the *XY*-plane, one could notice that we get an intensity distribution similarly to a Fresnel zone plate or Fraunhofer diffraction pattern from a circular aperture,[159] where a central bright ring (Figure 9c) is surrounded by darker (blue) ring.

Figure 9c shows the light propagation with the fundamental frequency (λ = 800 nm) through the hollow core of the FF-PNT, whereas the SHG light (λ_{SHG} = 400 nm) is generated and propagates in the noncentrosymmetric walls of the FF-PNT. The results demonstrate a good agreement between experimental observations and simulations.

The experimental data exhibit linear and nonlinear optical waveguiding in elongated peptide nanostructures. Compared to organic nanotubes[179] the bioinspired waveguiding peptide tubes are multifunctional: they reveal both nonlinear[44] and electro-optic[45] effects. Below we demonstrate bioinspired light waveguides which could be switched from passive regime to active one by reconformation of peptide secondary structure.[18]

5.2. Active Optical Peptide Waveguides

Passive waveguides directly guide the light beam through their optical transmission window. Its propagation is described by classical optical laws of reflection, refraction and diffraction. Compared to passive waveguiding the active one absorbs the input laser beam followed by excitation of FL signal and propagation of this fluorescence wave.[180,181] Guiding the excited fluorescence along the active waveguide was first revealed in organic dye nanofibers[182] and inorganic CdS nanowires.[180] The effect was ascribed to propagation of exciton–polaritons which are strongly coupled quasi-particles created between the laser-excited fluorescence and the material excitons.[181] Due to this completely different mechanism of the light propagation and strong optical confinement provided by high effective refractive index, active light waveguiding is observed in nanostructures with dimensions below diffraction limit[180,183–185] and enables the light propagation along ultrathin waveguides at macroscale length of hundreds micrometers and more.[181,182] These remarkable properties provide successful development of a new generation of nanophotonic devices including those which have acute bends of micrometer radius such as interferometers, couplers, and interconnectors.[182–187]

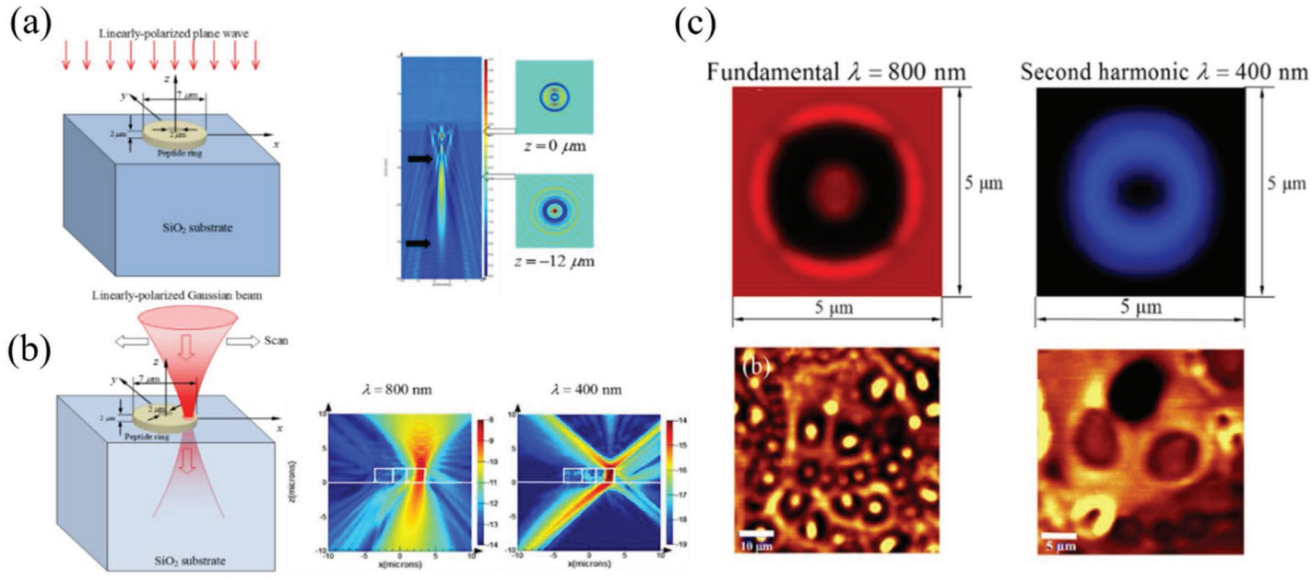

Figure 9. a) A plane wave impinges the vertically aligned FF-PNT formed by the breath figure method, and focuses in two points along the *Z*-axis. In the *XY*-plane, an intensity distribution like a Fresnel zone plate is observed. b) A Gaussian wave impinges the vertically aligned FF PNT, and passes through the core of the nanotube at fundamental frequency (800 nm) and generates SHG signal (400 nm) at the asymmetric crystalline clad. c) Upper row: simulated intensity distribution in the *XY*-plane at fundamental wavelength ($\lambda = 800$ nm) and at SHG wavelength ($\lambda = 400$ nm); lower row: experimental data: linear optical waveguiding ($\lambda = 800$ nm), and experimental SHG waveguiding ($\lambda = 400$ nm). Reproduced with permission.[48] Copyright 2016, Elsevier.

Active optical waveguides are fabricated from materials of different origin such as inorganic semiconductors,[180] dyes-doped polymer fibers,[187] organic crystals and nanofibers constructed from organic dyes[181,183] and luminescent molecules.[188] Waveguides with long-range propagation of exciton-polaritons in photoexcited fibers of thiacyanine dye[181,183,189–191] have been demonstrated (**Figure 10**a–c).

The same technique of incorporated fluorescent dye molecules was applied to bio-organic FF-peptide[46,192,193] and amyloid-inspired nanostructures[47] where organic fluorophores provided active waveguiding effect. Figure 10d–f demonstrates active waveguiding in elongated FF-peptide crystals.[194] It exhibits brighter FL emission (excitation by light $\lambda \approx 330$–380 nm) at the ends than that in the crystalline fiber. Figure 10e shows locally excited FL spot followed by FL wave propagation along the peptide waveguide which out-couples at its remote end as well active waveguiding of FL-excited wave in peptide structure doped by Nile Red dye.[194] Rod nanostructured assemblies of diphenylalanine, doped with Rhodamine B dye,[192] and ultralong aligned FF-dipeptide single crystals, doped by Rodhamine 6G dye,[195] have been demonstrated as active waveguides which can effectively confine and guide locally excited FL radiation.

Active optical waveguiding having completely different origin in FFF-peptide nanotapes was revealed in the work.[18] It is based on propagation of intrinsic visible FL in peptide nanostructures[53,196] Switching of the waveguiding mode from passive to active in peptide FFF-platelet structures was reported in the work.[18] Unlike active waveguiding in dyes-doped organic and bio-organic structures this new biophotonic broadband visible FL effect[53,196] does not involve an incorporation of foreign fluorescent dyes into original peptide material. The visible FL appears due to reconformation of peptide secondary structure from native state to β-sheet and is ascribed to the network of hydrogen bonds of this basic peptide/protein organization[18,53,119–121] (Figure 3).

Active waveguiding was also observed in FFF-nanofibers thermally grown from self-assembled FFF-peptide microspheres (**Figure 11**a–d). SEM microscopic images show native FFF-spheres with average size of about 5 μm (Figure 11a,b) which grew under gradual heating at $T \approx 160$–180 °C into hollow FFF-nanofibers (Figure 11c,d) having β-sheet secondary structure. When a heated FFF-sphere is illuminated by focused laser beam with the wavelength $\lambda = 405$ nm a strong broadband FL, excited in the spheres volume, propagates along the FFF-fiber and coupled-out from their ends. Visible FL microscopic images (Figure 11e–g) were captured through green, yellow and red filters correspondingly. Electromagnetic simulation and mode analysis of this structure showed that peptide nanofiber with inner and outer diameters of 500 and 800 nm, refractive index $n = 1.6$, placed in air environment, supports about 10 propagating modes at the wavelength 600 nm. It can be seen that this experimentally recorded pattern (Figure 11h) is similar to the intensity pattern (Figure 11h, inset) of one of the calculated modes (both of them have four intensity lobes).

It is interesting to estimate the possibility of active waveguiding in thermally treated peptide nanofibers in the framework of exciton–polariton model propagation, as it was demonstrated in thiacyanine dye fibers.[183,190,191] It was experimentally and theoretically proved[191] that exciton–polaritons-mediated active waveguiding is characterized by high effective refractive index and, consequently, by shorter wavelengths of waveguide modes in comparison with those in ordinary dielectric waveguides. This very important property makes it possible to fabricate very small, nearly subwavelength, integrated components for biocompatible photonic devices.

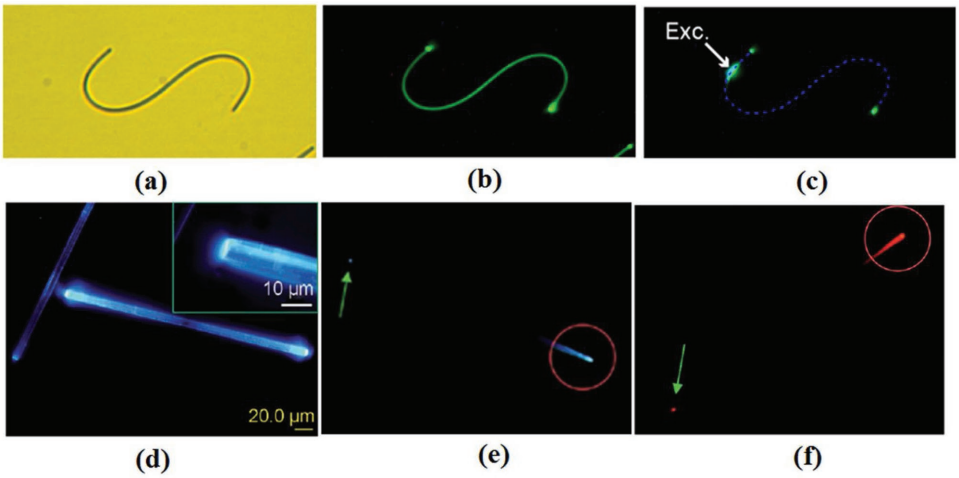

Figure 10. Active optical waveguides in organic fibers. a) Optical micrograph and b) FL microscopy image of the bent thiacyanine (TC) dye nanofiber on a glass substrate. The excitation and detection wavelength in the FL microscopy imaging were $\lambda < 475$ nm and $\lambda > 510$ nm, respectively. c) FL microscopy image of the bent nanofiber recorded by exciting the position labeled "Exc." with a focused laser beam ($\lambda = 405$ nm). Dashed line representing the nanofiber is an eye guide. a–c) Adapted with permission.[191] Copyright 2013, American Chemical Society. Active optical waveguides in bioinspired dyes-doped bio-organic peptide fibers. d) FL image of a single platelet showing brighter FL emission at the ends than in the fiber body; the inset shows magnified image of the FL at one end. e) Observation of waveguiding with local excitation at one end of an individual platelet. f) Waveguiding with local excitation of a platelet incorporating Nile Red dye. The red circle marks the excitation area, and the green arrow denotes the out-coupling of FL emission at the other end. d–f) Adapted with permission.[194] Copyright 2013, American Chemical Society.

Materials, exhibiting formation and propagation of exciton–polaritons, also demonstrate high optical absorption and high value of imaginary part of the complex refractive index. Local optical absorption spectrum of a few thermally treated β-sheet FFF-peptide tapes of 0.5–1 μm thick was measured by the use of microscopic spectrometer (**Figure 12**a). Then these data were used to calculate the spectrum of imaginary part of the complex refractive index (Figure 12b). We believe that optical absorption data from Figure 12a can also be applicable to thermally grown peptide β-sheet nanofibers presented above in Figure 11.

Figure 12b shows a low value of the imaginary part of complex refractive index in thermally treated peptide samples. Therefore, the contribution of exciton–polaritons propagation to active waveguiding in the experiment, presented in Figure 11, is relatively small. Consequently, in this experiment we observed a combination of active and passive waveguiding

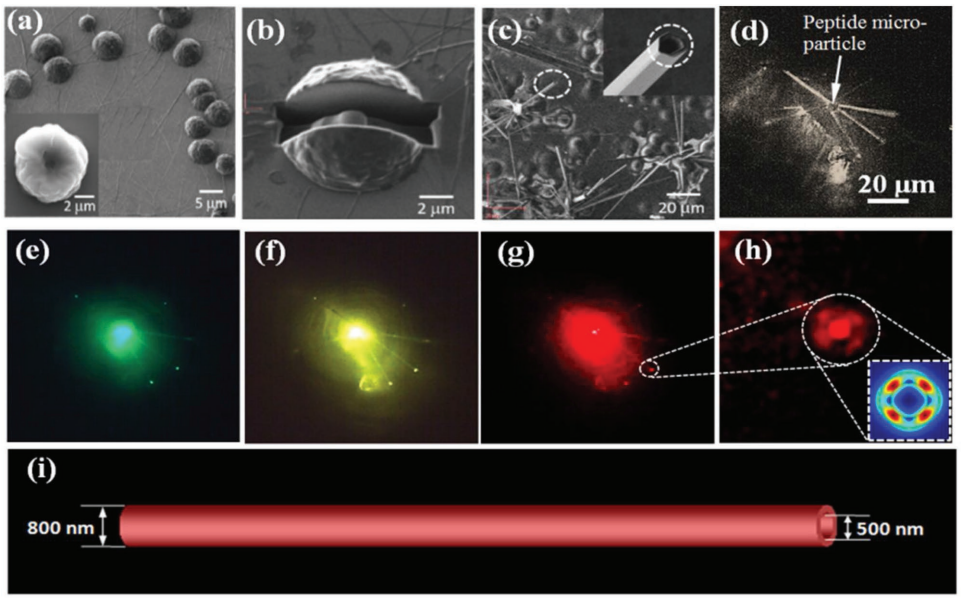

Figure 11. a) SEM image of FFF-nanospheres. b) SEM image of inner structure of FFF-nanosphere (FIB-etched). c) SEM image of FFF-nanofibers, grown from FFF-peptide microspheres, inset: FFF-nanofiber. d) Optical microscope image of the FFF-nanofibers. e–g) FL images of active optical waveguiding captured through green, yellow and red color filters. h) Experimental and simulated (inset) intensity pattern of waveguide mode. i) Geometry of simulated FFF-peptide nanofiber.

effect, in which the initial local excitation of FL radiation is also followed by its passive propagation due to the effective light confinement inside the dielectric peptide core.

To have a better insight into the physics, the optical modes supported by β-sheet peptide thin film was considered. It describes thin wall (≈100 nm thick) of the hollow fiber (≈1 μm diameter). The geometry is that of a thin parallel-sided slab of the thickness d specified by the dielectric function ε_1 and surrounded by semi-infinite media specified by the same ε_2 (Figure 12c). For the sake of simplicity relative magnetic permeability was taken equal to unity. The coordinate axes are chosen so that the Z axis is perpendicular to the interface with $z = 0$ is the plane of symmetry. The X axis is in the surface wave propagation direction while the orthogonal Y axis lies in the interface plane. Medium 2 is a pure nonabsorbing dielectric, $\varepsilon_2 > 0$, and medium 1 is a surface-active medium, $\varepsilon_1 = \varepsilon'_1 + i\varepsilon''_1$ ($\varepsilon''_1 < 0$). The space dependence of the fields in medium 2 is described by the term ~ exp $[i(k_x \pm k_{z2}z)]$ where signs "+" and "–" correspond to z > 0 and $z < 0$, respectively, and $k_x = k'_x + ik''_x$. Using the dispersion relation for the long-range mode[197] and under the assumption that thickness d is small, one gets that the term k''_x describing the surface mode decay in the X direction is proportional to small parameter $(k_0 d/2)^2 \ll 1$, i.e., in accordance with[197,198] $k''_x \sim k_0(k_0 d/2)^2 (-\varepsilon''_1) \ll k_0 (-\varepsilon''_1)$ where $k_0 = 2\pi/\lambda_0$ is the value of the wave number in vacuum. This defines a long-range propagation of the surface mode. Such a mode was predicted for the first time for a real metal where $\varepsilon'_1 < 0$ and $|\varepsilon'_1| \gg |\varepsilon''_1|$,[199] and later for an excitonic absorber where $\varepsilon'_1 = 0$ and $|\varepsilon''_1| > \varepsilon_2$ (long-range surface exciton–polariton).[200] For a dielectric with a weak absorption where $\varepsilon'_1 > 0$ and $|\varepsilon''_1| \ll \varepsilon'_1$, a normal strong TM guided mode is realized.[198] One can show that the last mode is not the surface mode. A similar mode is realized in our experiments, described in Figure 11, since the material parameters of β-sheet peptide fiber correspond to a dielectric with a weak absorption considered above.

6. Summary and Perspectives

In this work a new paradigm of bionanophotonics based on optical waveguiding in self-assembled 1D- and 2D-elongated peptide bioinspired nanostructures has been considered. The most distinguished feature of these emerging physics and technology of peptide optical materials, highlighted by us, is a thermally activated reconformation of their biological secondary structure from native phase to antiparallel β-sheet followed by formation of the fiber morphology. Such a reconstructive transition found in both aromatic and nonaromatic ultrashort di- and tripeptides is completely consistent with Dobson' theory when nondisease-related peptide/proteins can be converted to amyloid-like structures.[201,202] This biomolecular refolding of "amyloid" peptide nanostructure deeply modifies basic optical properties and optical waveguiding principles of the light propagation especially at the nanometer scale.

Two completely different modes of optical waveguiding in bioinspired nanostructures, passive and active, have been found. Passive waveguiding is observed in the native α-helical phase where optical transparency in a very wide range, pronounced nonlinear optical and electro-optical properties have enabled to fabricate and test a variety of multifunctional peptide integrated optical devices.

Active optical waveguiding has been found in "amyloid-like" nondisease peptide fiber nanostructures converted into β-sheet architecture where unknown previously effects of broadband optical absorption in the range 330–650 nm which is followed by tunable visible fluorescence have been observed. This intrinsic FL biophotonic effect is a common phenomenon and observed in any β-sheet structure from the simplest ultrashort peptides to neurogenerative protein fibrils and natural silk fibers. The dense network of noncovalent hydrogen bonds connecting β-strands motifs in the β-sheet structure of the peptide fibers is responsible for this new universal biophotonic effect.

Passive waveguiding is obeyed to the classical optical laws of reflection, refraction, and diffraction. The ideally lossless light wave propagates in its transmission window within native waveguides of a limited dimension $d > 0.5\lambda$. The revealed active light waveguiding is completely different. The input optical beam, launched into refolded β-sheet amyloid-like peptide waveguide, is absorbed just in the region, which is fully transparent in the native passive waveguides. This absorbed light flux excites the FL photons which can propagate in dozen of micrometer-long distances along thin peptide fibers of subwavelength thick below the diffraction limit.

Fine mechanism of a long-range FL propagation can be based on strong coupling between excitons and photons in a condensed matter. It results in the formation of new quasiparticles, exciton–polaritons (EPs), which combine exciton and photon properties.[180,181] Notable advance has been made

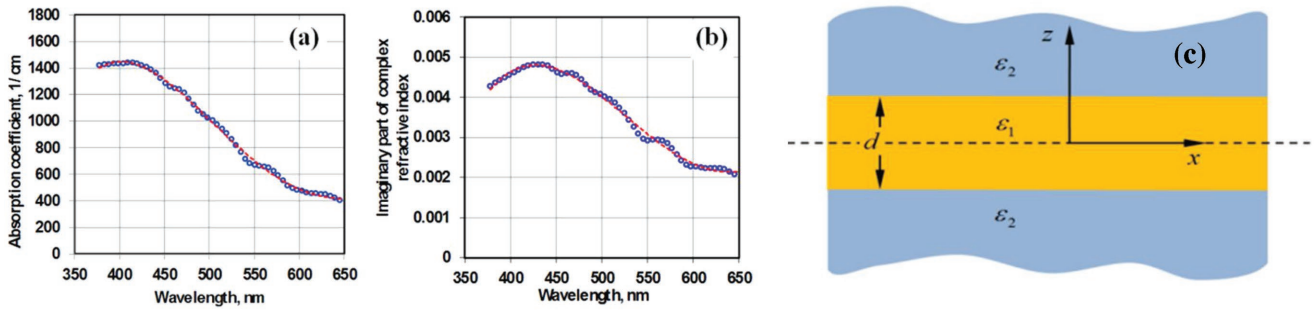

Figure 12. a) Spectrum of optical absorption coefficient in thermally treated β-sheet FFF-peptide nanostructure. b) Spectrum of the imaginary part of the complex refractive index in β-sheet FFF-peptide nanofibers. c) A thin parallel-sided slab of the thickness d specified by the dielectric function ε_1 and surrounded by semi-infinite media specified by the same ε_2 (symmetric case).

in Frenkel EPs in organic materials including long-range propagation of Frenkel EPs in dye-doped nanofibers at room temperature,[183] Frenkel EP lasers,[203,204] and Bose–Einstein condensation of Frenkel Eps.[205] In organic dyes nanofibers long-range Frenkel EPs are formed owing to a considerably larger oscillator strength compared to inorganic semiconductors. The oscillator strength of β-sheet peptide/protein fibers may be also very high and provide the long-range propagation of the Frenkel EPs.

Recently a mean-field electron-vibrational theory of Frenkel excitons[206] and EPs in organic dye structures[207] has been developed and applied to the experiments[181] indicating a good agreement between theory and experiment. In this relation it is worthy to note the advantage of normal strong TM guiding in a dielectric with weak absorption compared to long-ranging Frenkel EP. The point is that the latter is possible only for frequencies that are out of the absorption range and the splitting range between two branches of the polariton dispersion that shows also the leaky part in the splitting range.[207] In contrast, the decay of the normal strong TM mode observed in β-sheet nanofibers with higher optical absorption is proportional to a small parameter $(k_0 d/2)^2 \ll 1$ and can be made as small as needed by reducing the waveguiding wall thickness d.

Future theoretical and experimental research can give a deeper understanding of the physics of propagation of optical modes in peptide/protein ultrathin fibers. This emerging bionanophotonics of these peptide/protein bioinspired and biological nanofibrillar materials represents a great interest for a new generation of integrated biomedical nano-optics toward implantable lab-on-chips for health monitoring and new biomedical technology of light diagnostics, optogenetics, and precise phototherapy of ultrathin biological fibers and especially neurodegenerative disease-related amyloid fibrils.

Acknowledgements

This project was supported by Ministry of Science, Technology and Space of Israel.

Conflict of Interest

The authors declare no conflict of interest.

Keywords

beta-sheet visible fluorescence, implantable biochips, nonlinear optical and electrooptical effects, peptide nanophotonics, passive and active optical waveguides, reconformation of peptide secondary structure, switching of waveguiding regimes

Received: March 25, 2018
Revised: May 8, 2018
Published online:

[1] R. Hunsperger, *Integrated Optics: Theory and Technology*, Springer, Berlin **2009**.
[2] P. N. Prasad, *Nanophotonics*, John Willey & Sons, Inc., Hoboken, New Jersey, USA **2004**.
[3] H. J. Caulfield, S. Dolev, *Nat. Photonics* **2010**, *4*, 261.
[4] K. Tilbury, P. J. Campagnola, *Perspect. Med. Chem.* **2015**, *7*, PMC. S13214.
[5] X. Chen, O. Nadiarynkh, S. Plotnikov, P. J. Campagnola, *Nat. Protoc.* **2012**, *7*, 4, 655.
[6] R. LaComb, O. Nadiarnykh, S. S. Townsend, P. J. Campagnola, *Opt. Commun.* **2008**, *281*, 1823.
[7] R. Langert, *Science* **2001**, *293*, 5527, 58.
[8] M. Vanneman, G. Dranoff, *Nat. Rev. Cancer* **2012**, *12*, 237.
[9] S. H. Yun, S. J. J. Kwok, *Nat. Biomed. Eng.* **2017**, *1*, 0008.
[10] M. Humar, S. J. J. Kwok, M. Choi, S. Cho, A. K. Yetisen, S.-H. Yun, *Nanophotonics* **2016**, *5*, 60.
[11] A. Polosukhina, J. Litt, I. Tochitsky, J. Nemargut, Y. Sychev, I. De Kouchkovsky, T. Huang, K. Borges, D. Trauner, R. N. Van Gelder, R. H. Kramer, *Neuroendocrinology* **2012**, *75*, 271.
[12] L. M. Hadi, A. J. MacRobert, M. Loizidou, E. Yaghini, *Nanoscale* **2018**, *10*, 1570.
[13] N. R. Finsen, *Hospitalstidende* **1893**, *36*, 721.
[14] S. L. Jacques, *Phys. Med. Biol.* **2013**, *58*, R37.
[15] N. Paragios, J. Duncan, N. Ayache, *Handbook of Biomedical Imaging: Methodologies and Clinical Research*, Springer, USA **2014**.
[16] C. Bremer, V. Ntziachristos, R. Weissleder, *Eur. Radiol.* **2003**, *13*, 231.
[17] R. A. Robb, *Biomedical Imaging, Visualization, and Analysis*, John Wiley & Sons, Inc., New York **1999**.
[18] A. Handelman, N. Lapshina, B. Apter, G. Rosenman, *Adv. Mater.* **2018**, *30*, 1705776.
[19] M. Ghadiri, J. Grania, R. Milligan, D. McRee, N. Khazanovitch, *Nature* **1993**, *366*, 324.
[20] R. V. Ulijn, A. M. Smith, *Chem. Soc. Rev.* **2008**, *37*, 664.
[21] N. C. Seeman, A. M. Belche, *Proc. Natl. Acad. Sci. USA* **2002**, *99*, 6451
[22] B. Pokroy, S. H. Kang, L. Mahadevan, J. Aizenberg, *Science* **2009**, *323*, 237.
[23] S. Tadepalli, J. M. Slocik, M. K. Gupta, R. R. Naik, Sr. Singamanen, *Chem. Rev.* **2017**, *117*, 12705.
[24] R. Langer, D. A. Tirrell, *Nature* **2004**, *428*, 487.
[25] J. B. Matson, S. I. Stupp, *Chem. Commun.* **2012**, *48*, 26.
[26] S. Zhang, *Nat. Biotechnol.* **2003**, *21*, 1171.
[27] M. Reches, E. Gazit, *Science* **2003**, *300*, 625.
[28] P. Makam, E. Gazit, *Chem. Soc. Rev.* **2018**, *47*, 3406.
[29] L. Adler-Abramovich, D. Aronov, P. Beker, M. Yevnin, S. Stempler, L. Buzhansky, G. Rosenman, E. Gazit, *Nat. Nanotechnol.* **2009**, *4*, 849.
[30] L. Adler-Abramovich, E. Gazit, *Chem. Soc. Rev.* **2014**, *43*, 6881.
[31] A. Handelman, P. Beker, N. Amdursky, G. Rosenman, *Phys. Chem. Chem. Phys.* **2012**, *14*, 6391.
[32] A. Lakshmanan, C. A. E. Hauser, *Int. J. Mol. Sci.* **2011**, *12*, 5736.
[33] O. Silberbush, M. Amit, S. Roy, N. Ashkenasy, *Adv. Funct. Mater.* **2017**, *27*, 1604624.
[34] S. Subhra Panda, H. E. Katz, J. D. Tovar, *Chem. Soc. Rev.* **2018**, *47*, 3640.
[35] K. Tao, P. Makam, R. Aizen, E. Gazit, *Science* **2017**, *358*, eaam9756.
[36] V. Nguyen, S. Kelly, R. Yang, *APL Mater.* **2017**, *5*, 074108
[37] S. Safaryan, V. Slabov, S. Kopyl, K. Romanyuk, I. Bdikin, S. Vasilev, P. Zelenovskiy, V. Y. Shur, E. A. Uslamin, E. A. Pidko, A. V. Vinogradov, A. L. Kholkin, *ACS Appl. Mater. Interfaces* **2018**, *10*, 10543.
[38] S. Kim, J. H. Kim, J. S. Lee, C. B. Park, *Small* **2015**, *11*, 3623.
[39] I. Azuri, L. Adler-Abramovich, E. Gazit, O. Hod, L. Kronik, *J. Am. Chem. Soc.* **2014**, *136*, 963.
[40] X. Yan, Y. Su, J. Li, J. Fruh, H. Mohwald, *Angew. Chem., Int. Ed.* **2011**, *50*, 11186.
[41] A Handelman, B. Apter, T. Shostak, G. Rosenman, *J. Pept. Sci.* **2017**, *23*, 95.

[42] N. Amdursky, M. Molotskii, E. Gazit, G. Rosenman, *Appl. Phys. Lett.* **2009**, *94*, 261907.
[43] J. Ryu, S. Y. Lim, C. B. Park, *Adv. Mater.* **2009**, *21*, 1577.
[44] A. Handelman, S. Lavrov, A. Kudryavtsev, A. Khatchatouriants, Y. Rosenberg, E. Mishina, G. Rosenman, *Adv. Opt. Mater.* **2013**, *1*, 875.
[45] B. Gilboa, C. Lafargue, A. Handelman, L. J. W. Shimon, G. Rosenman, J. Zyss, T. Ellenbogen, *Adv. Sci.* **2017**, *4*, 1700052.
[46] X. Yan, J. Li, H. Möhwald, *Adv. Mater.* **2011**, *23*, 2796.
[47] W. Liyanage, N. M. B. Cogan, B. L. Nilsson, *ChemNanoMat* **2016**, *2*, 800.
[48] A. Handelman, B. Apter, N. Turko, G. Rosenman, *Acta Biomater.* **2016**, *30*, 72.
[49] X. Qiao, Z. Qian, J. Li, H. Sun, Y. Han, X. Xia, J. Zhou, C. Wang, Y. Wang, C. Wang, *ACS Appl. Mater. Interfaces* **2017**, *9*, 14665.
[50] B. D. Lawrence, M. Cronin-Golomb, I. Georgakoudi, D. L. Kaplan, F. G. Omenetto, *Biomacromolecules* **2008**, *9*, 1214.
[51] H. Tao, J. M. Kainerstorfer, S. M. Siebert, E. M. Pritchard, A. Sassaroli, B. J. B. Panilaitis, M. A. Brenckle, J. J. Amsden, J. Levitt, S. Fantini, D. L. Kaplan, F. G. Omenetto, *Proc. Natl. Acad. Sci. USA* **2012**, *109*, 19584.
[52] F. G. Omenetto, D. L. Kaplan, *Nat. Photonics* **2008**, *2*, 641.
[53] A. Handelman, N. Kuritz, A. Natan, G. Rosenman, *Langmuir* **2016**, *32*, 2847.
[54] E. A. Sykes, A. Albanese, W. C. Chan, *Nat. Photonics* **2013**, *7*, 940.
[55] W. F. Cheong, S. A. Prahl, A. Welch, *IEEE J. Quantum Electron.* **1990**, *26*, 2166.
[56] A. Canales, X. Jia, U. P. Froriep, C. M Tringides, J. Selvidge, C. Lu, C. Hou, L. Wei, Y. Fink, P. Anikeeva, *Nat. Biotechnol.* **2015**, *33*, 277.
[57] S. Nizamoglu, M. C. Gathe, M. Humar, M. Choi, S. Kim, K. S. Kim, S. K. Hahn, G. Scarcelli, M. Randolph, R. W. Redmond, S. H. Yun, *Nat. Commun.* **2016**, *7*, 10374.
[58] H. Lee, Y. Lee, C. Song, H. R. Cho, R. Ghaffari, T. K. Choi, K. H. Kim, Y. B. Lee, D. Ling, H. Lee, S. J. Yu, S. H. Choi, T. Hyeon, D.-H. Kim, *Nat. Commun.* **2015**, *6*, 1.
[59] S.-M. Park, A. Aalipour, O. Vermesh, J. Ho Yu, S. S. Gambhir, *Nat. Rev. Mater.* **2017**, *2*, 17014.
[60] R. Feiner, T. Dvir, *Nat. Rev. Mat.* **2017**, *3*, 17076.
[61] M. Kendall, I. Lynch, *Nat. Nanotechnol.* **2016**, *11*, 206.
[62] S. Lenhert, F. Brinkmann, T. Laue, S. Walheim, C. Vannahme, S. Klinkhammer, M. Xu, S. Sekula, T. Mappes, T. Schimmel, H. Fuchs, *Nat. Nanotechnol.* **2010**, *5*, 275.
[63] S. Carrara, S. Ghoreishizadeh, J. Olivo, I. Taurino, C. Baj-Rossi, A. Cavallini, M. Op de Beeck, C. Dehollain, W. Burleson, F. G. Moussy, A. Guiseppi-Elie, G. De Micheli, *Sensors* **2012**, *12* , 11013.
[64] F. Valgimigli, F. Lucarelli, C. Scuffi, S. Morandi, I. Sposato, *J. Diabetes Sci. Technol.* **2010**, *4*, 1182.
[65] B. Yu, N. Long, Y. Moussy, F. Moussy, *Biosens. Bioelectron.* **2006**, *21*, 2275.
[66] M. Choi, J. W. Choi, S. Kim, S. Nizamoglu, S. K. Hahn, S. H. Yun, *Nat. Photonics* **2013**, *7*, 12, 987.
[67] H. Perry, A. Gopinath, D. L. Kaplan, L. Dal Negro, F. G. Omenetto, *Adv. Mater.* **2008**, *20*, 3070.
[68] S. T. Parker, P. Domachuk, J. Amsden, J. Bressner, J. A. Lewis, D. L. Kaplan, F. G. Omenetto, *Adv. Mater.* **2009**, *21*, 2411.
[69] B. D. Ratner, A. S. Hoffman, F. Schoen, J. E. Lemons, *Biomaterials Science: An Introduction to Materials in Medicine*, Academic Press, Kidlington, Oxford, UK **2004**, pp. 162–164.
[70] M. Irimia-Vladu, *Chem. Soc. Rev.* **2014**, *43*, 588.
[71] S. Nair, C. T. Laurencin, *Prog. Polym. Sci.* **2007**, *32*, 762.
[72] A. S. Hoffman, *Adv. Drug Del. Rev.* **2002**, *64*, 3.
[73] M. Choi, J. W. Choi, S. Kim, S. Nizamoglu, S. K. Hahn, S. H. Yun, *Nat. Photonics* **2013**, *7*, 987.
[74] J. Kim, S. Kwon, S. H. Kim, C. K. Lee, J. H. Lee, S. J. Cho, H. S. Lee, H. Ihee, *J. Am. Chem. Soc.* **2012**, *134*, 20573.
[75] S. Kwon, B. J. Kim, H. K. Lim, K. Kang, S. H. Yoo, J. Gong, E. Yoon, J. Lee, I. Choi, H. Kim, H. S. Lee, *Nat. Commun.* **2015**, *6*, 874.
[76] M. Reches, E. Gazit, *Nat. Nanotechnol.* **2006**, *1*, 195.
[77] A. Kholkin, N. Amdursky, I. Bdikin, E. Gazit, G. Rosenman, *ACS Nano* **2010**, *4*, 610.
[78] J. S. Lee, I. Yoon, J. Kim, H. Ihee, B. Kim, C. B. Park, *Angew. Chem., Int. Ed.* **2011**, *50*, 1164.
[79] L. Adler-Abramovich, N. Kol, I. Yanai, D. Barlam, R. Z. Shneck, E. Gazit, I. Rousso, *Angew. Chem., Int. Ed.* **2010**, *49*, 9939.
[80] V. L. Sedman, X. Chen, S. Allen, C. J. Roberts, V. V. Korolkov, S. J. B. Tendler, *J. Microsc.* **2013**, *249*, 165.
[81] N. Amdursky, E. Gazit, G. Rosenman, *Biochem. Biophys. Res. Commun.* **2012**, *419*, 232.
[82] N. Amdursky, E. Gazit, G. Rosenman, *Adv. Mater.* **2010**, *22*, 2311.
[83] N. Amdursky, G. Shalev, A. Handelman, S. Litsyn, A. Natan, Y. Roizin, Y. Rosenwaks, D. Szwarcman, G. Rosenman, *APL Matter.* **2013**, *1*, 062104.
[84] Y. Ikezoe, G. Washino, T. Uemura, S. Kitagawa, H. Matsui, *Nat. Mater.* **2012**, *11*, 1081.
[85] V. Nguyen, R. Zuo, K. Jenkins, R. Yang, *Nat. Commun.* **2016**, *7*, 13566.
[86] X. Yan, Q. He, K. Wang, L. Duan, Y. Cui, J. Li, *Angew. Chem., Int. Ed.* **2007**, *46*, 2431.
[87] K. H. Smith, E. Tejeda-Montes, M. Poch, A. Mata, *Chem. Soc. Rev.* **2011**, *40*, 4563.
[88] K. Matsuurua, *RSC Adv.* **2014**, *4*, 2942.
[89] T. Han, J. Kim, J. S Park, C. B. Park, H. Ihee, S. O. Kim, *Adv. Mater.* **2007**, *19*, 3924.
[90] V. Nguyen, K. Jenkins, R. Yang, *Nano Energy* **2015**, *17*, 323.
[91] M. Wang, L. Du, X. Wu, S. Xiong, P. K. Chu, *ACS Nano* **2011**, *5*, 4448.
[92] R. J. A. Hill, V. L. Sedman, S. Allen, P. M, . Williams, M. Paoli, L. Adler-Abramovich, E. Gazit, L. Eaves, S. J. B. Tendler, *Adv. Mater.* **2007**, *19*, 4474.
[93] Z. A. Arnon, A. Vitalis, A. Levin, T. C. T. Michaels, A. Caflisch, T. P. J. Knowles, L. Adler-Abramovich, E. Gazit, *Nat. Commun.* **2016**, *7*, 13190.
[94] J. Chen, S. Qin, X. Wu, A. P. Chu, *ACS Nano* **2016**, *10*, 832.
[95] D. Aronov, L. Adler-Abramovich, E. Gazit, G. Rosenman, *J. Nanosci. Nanotechnol.* **2008**, *8*, 1.
[96] G. Singh, A. M. Bittner, S. Loscher, N. Malinowski, K. Kern. *Adv. Mater.* **2008**, *20*, 2332.
[97] H. Taha, R. S. Marks, L. A. Gheber, I. Rousso, J. Newman, C. Sukenik, A. Lewis, *Appl. Phys. Lett.* **2003**, *83*, 1041.
[98] M. Sokuler, L. A. Gheber, *Nano Lett.* **2006**, *6*, 848.
[99] N. Amdursky, E. Gazit, M. Molotskii, G. Rosenman, *J. Am. Chem. Soc.* **2010**, *132*, 15632.
[100] C. B. Anfinsen, *Science* **1973**, *181*, 223.
[101] J. A. Schellman, C. G. Schellman, *Protein Sci.* **1997**, *6*, 1092.
[102] E. D. Eanes, G. G. Glenner, J. Histochem, *J. Histochem. Cytochem.* **1968**, *16*, 673.
[103] C. M. Dobson, *Nature* **2003**, *426*, 884.
[104] H. Mihara, Y. Takahashi, *Curr. Opin. Struct. Biol.* **1997**, *7*, 501.
[105] C. A. E. Hauser, R. Deng, A. Mishra, Y. Loo, U. Khoe, F. Zhuang, D. W. Cheong, A. Accardo, M. B. Sullivan, C. Riekel, J. Y. Ying, U. A. Hauser, *Proc. Natl. Acad. Sci. USA* **2011**, *108*, 1361.
[106] C. M. Dobson, *Philos. Trans. R. Soc., B* **2001**, *356*, 133.
[107] F. Chiti, C. M. Dobson, *Annu. Rev. Biochem.* **2006**, *75*, 333.
[108] E. Gazit, *Angew. Chem., Int. Ed.* **2002**, *41*, 257.
[109] T. P. J. Knowles, M. Vendruscolo, C. M. Dobson, *Phys. Today* **2015**, *68*, 36.
[110] G. U. Nienhaus, *Angew. Chem., Int. Ed.* **2008**, *47*, 8992.
[111] J. R. Lakowicz, *Principles of Fluorescence Spectroscopy*, Plenum Press, NY, USA **1983**.
[112] R. F. J. Chen, *J. Res. Natl. Bur. Stand., Sect. A* **1972**, *76A*, 593,

[113] T. Inagaki, *Biopolymers* **1973**, *12*, 1353.
[114] A. Handelman, A. Natan, G. Rosenman, *J. Pept. Sci.* **2014**, *20*, 487.
[115] N. Amdursky, P. Beker, I. Koren, B. Bank-Srour, E. Mishina, S. Semin, T. Rasing, Y. Rosenberg, Z. Barkay, E. Gazit, G. Rosenman, *Biomacromolecules* **2011**, *12*, 1349.
[116] C. Diaferia, T. Sibillano, N. Balasco, C. Giannini, V. Roviello, L. Vitagliano, G. Morelli, A. Accardo, *Chem. – Eur. J.* **2016**, *22*, 16586.
[117] C. Diaferia, T. Sibillano, N. Balasco, C. Giannini, V. Roviello, L. Vitagliano, G. Morelli, A. Accardo, *Chem. Eur J.* **2017**, *23*, 14309.
[118] R. Ye, Y. Liu, H. Zhang, H. Su, Y. Zhang, L. Xu, R. Hu, R. T. K. Kwok, K. S. Wong, J. W. Y. Lam, W. A. Goddard, B. Z. Tang, *Polym. Chem.* **2017**, *8*, 1722.
[119] F. T. Chan, G. S. Kaminski, J. R. Kumita, C. W. Bertoncini, C. M. Dobson, C. F. Kaminski, *Analyst* **2013**, *138*, 2156.
[120] C. F. Kaminski, G. S. Kaminski-Schierle, *Neurophotonics* **2016**, *3*, 041807.
[121] U. Shimanovich, D. Pinotsi, K. Shimanovich, N. Yu, S. Bolisetty, J. Adamcik, R. Mezzenga, J. Charmet, F. Vollrath, E. Gazit, C. M. Dobson, G. Kaminski Schierle, C. Holland, C. F. Kaminski, T. P. J. Knowles, *Macromol. Biosci.* **2018**, *18*, 1700295.
[122] D. Pinotsi, L. Grisanti, P. Mahou, R. Gebauer, C. F. Kaminski, A. Hassanali, G. S. Kaminski Schierle, *J. Am. Chem. Soc.* **2016**, *138*, 3046.
[123] L. Pasteur, C. R. Séances, *Acad. Sci.* **1848**, *26*, 538.
[124] C. Kittel, *Introduction to Solid State Physics*, 8th ed., John Wiley & Sons, USA **2005**.
[125] K. Yu, A. Panfilov, V. Smirnov, P. Tronc, *Phys. Rev. E* **2003**, *67*, 011907.
[126] V. V. Lemanov, S. N. Popov, G. A. Pankova, *Ferroelectrics* **2003**, *285*, 581.
[127] C. Harnagea, M. Vallieres, C. Pfeffer, D. Wu, B. Olsen, A. Pignolet, F. Legare, A. Gruverman, *Biophys. J.* **2010**, *98*, 3070.
[128] M. Nikiforov, G. Thompson, V. Reukov, S. Jesse, S. Guo, B. Rodriguez, K. Seal, A. Vertegel, S. Kalinin, *ACS Nano* **2010**, *4*, 689.
[129] M. Minary Jolandan, M. Feng Yu, *Nanotechnology* **2009**, *20*, 085706.
[130] E. Fukada, I. Yasuda, *Jpn. J. Appl. Phys.* **1964**, *3*, 117.
[131] A. Gruverman, B. J. Rodriguez, S. V. Kalinin, *Electromechanical Behavior in Biological Systems at the Nanoscale*, Springer, New York **2007**.
[132] S. B. Lang, *Nature* **1966**, *212*, 704.
[133] S. Psilodimitrakopoulos, S. I. C. O. Santos, I. Amat-Roldan, A. K. N. Thayil, D. Artigas, P. Loza-Alvarez, *J. Biomed. Opt.* **2009**, *14*, 014001.
[134] C. H. Gorbitz, *Chem. – Eur. J.* **2007**, *13*, 1022.
[135] G. R. Desiraju, *J. Am. Chem. Soc.* **2013**, *135*, 9952.
[136] G. Rosenman, P. Beker, I. Koren, M. Yevnin, B. Bank-Srour, E. Mishina, S. Semin, *J. Pept. Sci.* **2010**, *17*, 2, 75.
[137] R. W. Boyd, *Nonlinear Optics*, 3rd ed., Elsevier, San Diago, USA **2008**.
[138] L. M. Haupert, G J. Simpson, *Annu. Rev. Phys. Chem.* **2009**, *60*, 345.
[139] X. Chen, O. Nadiarynkh, S. Plotnikov, P. J. Campagnola, *Nat. Protoc.* **2012**, *7*, 654.
[140] T. Hompland, A. Erikson, M. Lindgren, T. Lindmo, C. Davies,L. de, *J. Biomed. Opt.* **2008**, *13*, 054050.
[141] Y. Ling, C. Li, K. Feng, S. Palmer, P. L. Appleton, S. Lang, D. McGloin, Z. Huang, G. Nabi, *J. Biophotonics* **2017**, *10*, 911.
[142] K. B. Tilbury, K. R. Campbell, K. W. Eliceiri, S. M. Salih, M. Patankar, P. J. Campagnola, *BMC Cancer* **2017**, *17*, 102.
[143] A. Finnøy, K. Olstad, M. B. Lilledahl, *BMC Vet. Res.* **2017**, *13*, 270.
[144] M. Hana, G. Giese, J. F. Bille, *Opt. Exp.* **2005**, *13*, 5791
[145] S. G. Stanciu, *Microscopy and Analysis*, Chapter 5, InTech, **2016**.
[146] D. J. Brown, N. Morishiqe, A. Neekhra, D. S. Minckler, J. V. Jester, *J. Biomed. Opt.* **2007**, *12*, 024029.
[147] S.-J. Lin, R.-J. Wu, H.-Y. Tan, W. Lo, W.-C. Lin, T.-H. Young, C.-J. Hsu, J.-S. Chen, S.-H. Jee, C.-Y. Dong, *Opt. Lett.* **2005**, *30*, 2275.
[148] F. Tiaho, G. Recher, D. Rouede, *Opt. Express* **2007**, *15*, 12286.
[149] S. Brasselet, *Adv. Opt. Photonics* **2011**, *3*, 205.
[150] S. Bancelin, C. Aimé, I. Gusachenko, L. Kowalczuk, G. Latour, T. Coradin, M.-C S. Klein, *Nat. Commun.* **2014**, *4920*, 1.
[151] I. Gusachenko, G. Latour, M.-C. Schanne-Klein, *Opt. Express* **2010**, *18*, 19339.
[152] C. Odin, T. Guilbert, A. Alkilani, O. P. Boryskina, V. Fleury, Y. Le Grand, *Opt. Express* **2008**, *16*, 16151.
[153] R M. Williams, W R. Zipfel, W. W. Webb, *Biophys. J.* **2005**, *88*, 1377.
[154] D. Aït-Belkacem, A. Gasecka, F. Munhoz, S. Brustlein, S. Brasselet, *Opt. Express* **2010**, *18*, 14859.
[155] F. Vanzi, L. Sacconi, R. Cicchi, F. S. Pavone, *J. Biomed. Opt.* **2012**, *17*, 060901.
[156] S. Roth, I. Freund, *J. Chem. Phys.* **1979**, *70*, 1637.
[157] S. Brasselet, V. L. Floc'h, F. Treussart, J. F. Roch, J. Zyss, E. Botzung-Appert, A. Ibanez, *Phys. Rev. Lett.* **2004**, *92*, 207401.
[158] S. Khanra, K. Ghosh, F. F. Ferreira, W. A. Alves, F. Punzo, P. Yu, S. Guha, *Phys. Chem. Chem. Phys.* **2017**, *19*, 3084.
[159] M. C. Teich, B. E. A. Saleh, *Fundamentals of Photonics*, Wiley, New York **1991**
[160] M. Sigelle, R. Hierle, *J. Appl. Phys.* **1981**, *52*, 4199.
[161] J. Clark, G. Lanzani, *Nat. Photonics* **2010**, *4*, 438.
[162] T. Yoshimura, *Thin-Film Organic Photonics. Molecular Layer Deposition and Applications*, CRC Press, Boca Raton, FL **2011**.
[163] R. G. Hunsperger, A. Yariv, A. Lee, *Appl. Opt.* **1977**, *16*, 1026.
[164] J. C. Campbell, *Appl. Opt.* **1979**, *18*, 2037.
[165] W. L. Emkey, *J. Lightwave Technol.* **1983**, *1*, 436.
[166] E. M. Zolotov, V. M. Pelekhatyi, *Sov. J. Quantum Electron.* **1974**, *4*, 542.
[167] J. F. Revelli, D. Sarid, *J. Appl. Phys.* **1980**, *51*, 3566.
[168] W. A. Pasmooij, P. A. Mandersloot, M. K. Smit, *J. Lightwave Technol.* **1989**, *7*, 175.
[169] N. Chandrasekhar, R. Chandrasekar, *Angew. Chem., Int. Ed.* **2012**, *51*, 3556.
[170] N. Chandrasekhar, Md A. Mohiddon, R. Chandrasekar, *Adv. Opt. Mater.* **2013**, *1*, 305.
[171] P. Hui, R. Chandrasekar, *Adv. Mater.* **2013**, *25*, 2963.
[172] S. Basak, R. Chandrasekar, *J. Mater. Chem. C* **2014**, *2*, 1404.
[173] Lumerical Inc., http://www.lumerical.com/tcad-products/fdtd/, (accessed: October 2016).
[174] Y.-S. Zhao, H. Fu, A. Peng, Y. Ma, Q. Liao, J. Yao, *Acc. Chem. Res.* **2010**, *43*, 409.
[175] M. Cazzanelli, F. Bianco, E. Borga, G. Pucker, M. Ghulinyan, E. Degoli, E. Luppi, V. Véniard, S. Ossicini, D. Modotto, S. Wabnitz, R. Pierobon, L. Pavesi, *Nat. Mater.* **2012**, *11*, 148.
[176] H. Zhang, Q. Liao, X. Wang, Z. Xu, H. Fu, *Nanoscale* **2015**, *7*, 10186.
[177] J. Xu, S. Semin, D. Niedzialek, P. H. J. Kouwer, E. Fron, E. Coutino, M. Savoini, Y. Li, J. Hofkens, H. U. D. Beljonne, T. Rasing, A. E. Rowan, *Adv. Mater.* **2013**, *25*, 2084.
[178] M. Du, P. Zhu, X. Yan, Y. Su, W. Song, J. Li, *Chem. – Eur. J.* **2011**, *17*: 4238.
[179] D. O'Carroll, I. Lieberwirth, G. Redmond, *Nat. Nanotechnol.* **2007**, *2*, 180.
[180] C. J. Barrelet, A. B. Greytak, C. M. Lieber, *Nano Lett.* **2004**, *4*, 1981.
[181] K. Takazawa, J. Inoue, K. Mitsuishi, T. Takamasu, *Phys. Rev. Lett.* **2010**, *105*, 067401.
[182] Y. S. Zhao, H. Fu, A. Peng, Y. Ma, D. Xiao, J. Yao, *Adv. Mater.* **2008**, *20*, 2859.

[183] K. Takazawa, J.-i. Inoue, K. Mitsuishi, T. Kuroda, *Adv. Funct. Mater.* **2013**, *23*, 839.
[184] R. Chandrasekar, *Phys. Chem. Chem. Phys.* **2014**, *16*, 7173.
[185] W. Zhang, Y. Sheng Zhao, *Chem. Commun.* **2016**, *52*, 8906.
[186] W. Yao, Y. Yan, L. Xue, C. Zhang, G. Li, Q. Zheng, Y. S. Zhao, H. Jiang, J. Yao, *Angew. Chem., Int. Ed.* **2013**, *52*, 8713.
[187] C. Zhang, Y. Yan, J. Yao, Y. S. Zhao, *Adv. Mater.* **2013**, *25*, 2854.
[188] C. Zhang, Y. S. Zhao, J. N. Yao, *Phys. Chem. Chem. Phys.* **2011**, *13*, 9060.
[189] K. Takazawa, Y. Kitahama, Y. Kimura, G. Kido, *Nano Lett.* **2005**, *5*, 1293.
[190] K. Takazawa, *J. Phys. Chem. C* **2007**, *111*, 8671.
[191] K. Takazawa, J.-I. Inoue, K. Mitsuishi, *ACS Appl. Mater. Interfaces* **2013**, *5*, 6182.
[192] Q. Li, Y. Jia, L. Dai, Y. Yang, J. Li, *ACS Nano* **2015**, *9*, 2689.
[193] Y. Li, L. Yan, K. Liu, J. Wang, A. Wang, S. Bai, X. Yan, *Small* **2016**, *12*, 2575.
[194] X. Yan, Y. Su, J. Li, J. Fruh, H. Möhwald, *Angew. Chem., Int. Ed.* **2011**, *50*, 11186.
[195] B. Sun, Q. Li, H. Riegler, S. Eickelmann, L. Dai, Y. Yang, R. Perez-Garcia, Y. Jia, G. Chen, J. Fei, K. Holmberg, J. Li, *ACS Nano* **2017**, *11*, 10489.
[196] N. Amdursky, M. Molotskii, D. Aronov, L. Adler-Abramovich, E. Gazit, G. Rosenman, *Nano Lett.* **2009**, *9*, 3111.
[197] H. Raether, *Surface Plasmons on Smooth and Rough Surfaces and on Gratings*, Springer-Verlag, Berlin **1986**
[198] F. Yang, J. R. Sambles, G. W. Bradberry, *Phys. Rev. B* **1990**, *44*, 5855.
[199] D. Sarid, *Phys. Rev. Lett.* **1981**, *47*, 1927.
[200] F. Yang, J. R. Sambles, G. W. Bradberry, *Phys. Rev. Lett.* **1990**, *64*, 559.
[201] J. I. Guijarro, M. Sunde, J. A. Jones, I. D. Campbell, C. M. Dobson, *Proc. Natl. Acad. Sci. USA* **1998**, *95*, 4224.
[202] G. Wei, Z. Su, N. P. Reynolds, P. Arosio, I. W. Hamley, E. Gazit, R. Mezzenga, *Chem. Soc. Rev.* **2017**, *46*, 4661.
[203] Q. Liao, Z. Xu, X. Zhong, W. Dang, Q. Shi, C. Zhang, Y. Weng, Z. Lid, H. Fu, *J. Mater. Chem. C* **2014**, *2*, 2773.
[204] C. P. Dietrich, A. Steude, L. Tropf, M. Schubert, N. M. Kronenberg, K. Ostermann, S. Hofling, M. C. Gather, *Sci. Adv.* **2016**, *2*, e1600666.
[205] J. D. Plumhof, T. Stoferle, L. Mai, U. Scherf, R. F. Mahrt, *Nat. Mater.* **2014**, *13*, 247.
[206] B. D. Fainberg, N. N. Rosanov, N. A. Veretenov, B. Apter, *Proc. SPIE* **2017**, *10360*, 1036003
[207] B. Fainberg, *Proc. 9th Int. Conf. on Metamaterials, Photonic Crystals and Plasmonics*, META'18, Marseille, France **2018**, Paper ID 723024.